Article

Current Biology

Dynamic remodeling of actin networks by cyclase-associated protein and CAP-Abp1 complexes

Graphical abstract

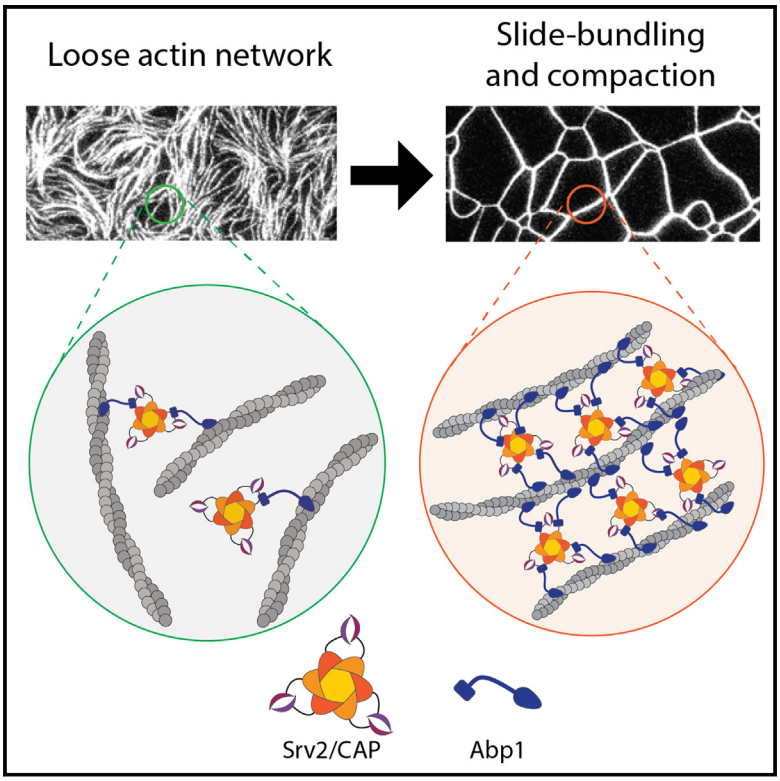

Highlights

- CAP and CAP-Abp1 complexes drive actin filament sliding, bundling, and coalescence
- CAP and Abp1 molecules accumulate where actin filaments overlap
- Disrupting CAP-Abp1 interactions causes actin organization defects *in vivo*

Authors

Siyang Guo, Gregory J. Hoeprich, Joseph O. Magliozzi, Jeff Gelles, Bruce L. Goode

Correspondence

gelles@brandes.edu (J.G.), goode@brandeis.edu (B.L.G.)

In brief

Guo et al. show that oligomeric cyclase-associated protein (CAP), enhanced by its binding partner Abp1, promotes the sliding, bundling, and coalescence of actin filaments, converting loose, unbranched (or branched) filaments into compact bundles.

Guo et al., 2023, Current Biology *33*, 4484–4495
October 23, 2023
https://doi.org/10.1016/j.cub.2023.09.032

CellPress

CellPress
OPEN ACCESS

Current Biology

Article

Dynamic remodeling of actin networks by cyclase-associated protein and CAP-Abp1 complexes

Siyang Guo,[1] Gregory J. Hoeprich,[1] Joseph O. Magliozzi,[1] Jeff Gelles,[2,*] and Bruce L. Goode[1,3,*]
[1]Department of Biology, Brandeis University, 415 South Street, Waltham, MA 02454, USA
[2]Department of Biochemistry, Brandeis University, 415 South Street, Waltham, MA 02454, USA
[3]Lead contact
*Correspondence: gelles@brandes.edu (J.G.), goode@brandeis.edu (B.L.G.)
https://doi.org/10.1016/j.cub.2023.09.032

SUMMARY

How actin filaments are spatially organized and remodeled into diverse higher-order networks *in vivo* is still not well understood. Here, we report an unexpected F-actin "coalescence" activity driven by cyclase-associated protein (CAP) and enhanced by its interactions with actin-binding protein 1 (Abp1). We directly observe *S. cerevisiae* CAP and Abp1 rapidly transforming branched or linear actin networks by bundling and sliding filaments past each other, maximizing filament overlap, and promoting compaction into bundles. This activity does not require ATP and is conserved, as similar behaviors are observed for the mammalian homologs of CAP and Abp1. Coalescence depends on the CAP oligomerization domain but not the helical folded domain (HFD) that mediates its functions in F-actin severing and depolymerization. Coalescence by CAP-Abp1 further depends on interactions between CAP and Abp1 and interactions between Abp1 and F-actin. Our results are consistent with a mechanism in which the formation of energetically favorable sliding CAP and CAP-Abp1 crosslinks drives F-actin bundle compaction. Roles for CAP and CAP-Abp1 in actin remodeling *in vivo* are supported by strong phenotypes arising from deletion of the CAP oligomerization domain and by genetic interactions between *sac6Δ* and an *srv2-301* mutant that does not bind Abp1. Together, these observations identify a new actin filament remodeling function for CAP, which is further enhanced by its direct interactions with Abp1.

INTRODUCTION

Cellular actin networks have diverse architectures tailored to their specific biological roles. For instance, filopodia consist of tightly packed parallel bundles of long filaments, lamellipodia consist of a dense meshwork of highly branched short filaments, and sarcomeres consist of long, highly ordered arrays of filaments with uniform length and spacing. Some aspects of these different spatial arrangements in actin networks arise from the actin nucleation and elongation factors involved in their assembly. The Arp2/3 complex nucleates branched actin networks, while formins polymerize unbranched filaments found in filopodia, stereocilia, stress fibers, polarized cables, and sarcomeres.[1–4] Organization of unbranched, or possibly debranched, linear actin filaments into higher order networks with specific geometries depends on a number of different crosslinking proteins with diverse properties. For example, fascin, α-actinin, and fimbrin organize filaments into parallel or anti-parallel bundles, whereas spectrin and filamin organize filaments into orthogonal arrays.[5] Together with the actin nucleation and elongation machinery, crosslinking/bundling proteins give actin networks their unique architectural organization, imbuing them with distinct physical properties that facilitate their biological functions.

Cellular actin networks also can be dynamically remodeled, both during and after they perform their biological functions. For instance, lamellipodial actin networks are initially assembled at the leading edge as highly branched arrays with specific mechanical properties optimized for membrane protrusion,[6] but then are rapidly pruned and repurposed as they move inward (away from the leading edge) in treadmilling networks.[7] Further, ventral stress fibers initially form as long bundles of filaments polymerized by formins at the leading edge, then collapse inward, rotating 90°, and are transformed into myosin-decorated contractile structures.[8,9] Similarly, remodeling of filamentous actin architecture occurs at sites of endocytosis, reshaping the actin network for optimal force generation as the membrane progressively invaginates and vesicles form.[10–12] At a molecular level, how cells control these and other dynamic rearrangements of filamentous actin arrays is only beginning to be understood.

Srv2/CAP was first identified in *S. cerevisiae*, both as a suppressor of Ras2, and thus named "suppressor of Ras valine 2" (Srv2), and as a protein associated with adenylate cyclase, thus named "cyclase-associated protein" (CAP).[13,14] Srv2/CAP is a 57 kDa actin-binding protein that is conserved across the animal, fungal, and plant kingdoms and plays important roles in promoting actin turnover.[15] The N-terminal half of *S. cerevisiae* and mouse Srv2/CAP proteins self-assemble into hexameric

bladed structures with 6-fold symmetry.[16,17] However, recent studies suggest that the oligomerization state of Srv2/CAP may be variable, and possibly species-specific, with some CAP proteins being reported to form tetramers and/or pentamers.[18,19] Regardless, in all cases tested, oligomerization requires the N-terminal oligomerization domain (OD), and the blades of the oligomeric structures are formed by the helical folded domains (HFDs), which are α helix bundles.[20–24] The Srv2/CAP shurikens bind transiently to F-actin sides (K_D = 1–8 μM) to enhance cofilin-mediated severing[17] and more strongly to the pointed ends of actin filaments, where they synergize with cofilin and twinfilin to accelerate pointed-end depolymerization.[25–28] In contrast, the C-terminal half of Srv2/CAP consists of an actin-binding WASP-homology 2 (WH2) domain, flanked by two proline-rich motifs (P1 and P2) and a β sheet/CARP (CAPs and X-linked retinitis pigmentosa 2) domain.[29] The WH2 domain binds to ATP- and ADP-actin monomers with similar affinity ($K_D \sim 1$ μM), while the CARP domain binds preferentially to monomeric ADP-actin ($K_D \sim 1.5$ μM).[22,30] Together, the WH2 and CARP domains catalyze the dissociation of cofilin and promote nucleotide exchange on ADP-actin monomers, recycling monomers back to an ATP-bound assembly competent state.[25,27,28] Consistent with these *in vitro* activities, *srv2Δ* mutants in *S. cerevisiae* exhibit severe defects in cell growth and morphology and reduced rates of endocytosis and cortical actin patch turnover.[16,23,31,32] Further, CAP disruptions in *C. elegans* and mammalian cells result in pronounced defects in actin cytoskeleton organization (including sarcomeres), endocytosis and cell motility, and physiological fitness.[20,33–35]

Actin-binding protein 1, or Abp1 (also known as HIP55, SH3P7, and Drebrin-like protein in mammalian systems), is a widely conserved and ubiquitously expressed protein with an N-terminal actin depolymerization factor homology (ADF-H) domain that binds F-actin.[36–39] Abp1 also has a C-terminal SH3 domain, which in *S. cerevisiae* Abp1 binds to Srv2/CAP, Ark1 and Prk1 kinases, and Scp1/Calponin.[40–43] The SH3 domain of Abp1 interacts with the proline-rich "P2" motif in Srv2/CAP.[40,44] Srv2's localization to endocytic actin patches is diminished by disruption of this interaction or *abp1Δ*.[32] Similarly, in mammalian cells, Abp1 and Srv2/CAP co-decorate many of the same actin structures and both proteins play important roles in endocytosis.[20,33–35]

Although the biochemical effects of Srv2/CAP and Abp1 have been studied individually, virtually nothing is known about their combined activities or the significance of their physical interaction. One of the few clues to a joint function for Srv2/CAP and Abp1 is a long-standing genetic observation made in yeast that *abp1Δ* and *srv2Δ* mutations are each synthetic lethal with mutations in fimbrin/Sac6 (*sac6Δ*).[45–47] Fimbrin/Sac6 (also called plastin) is a conserved F-actin bundling protein that decorates many cellular actin structures, including microvilli, filopodia, and stereocilia, and yeast endocytic actin patches.[48–51] In *S. cerevisiae*, *sac6Δ* cells exhibit defects in endocytosis, actin patch polarization and dynamics, and actin cable organization.[32,49,52,53] The observation that Srv2/CAP and Abp1 each share an essential function with Sac6/fimbrin raises the intriguing possibility that Srv2/CAP and Abp1 play roles in regulating the spatial organization of actin filaments.

In the present study, we investigate this possibility using total internal reflection fluorescence (TIRF) microscopy and directly observe Srv2/CAP promoting a novel form of actin network remodeling, which is enhanced by the Srv2/CAP association with Abp1. This activity is characterized by rapid sliding and coalescence of loose networks of actin filaments (branched or unbranched) into short, compact bundles. Multi-color single-molecule imaging reveals that Srv2/CAP and Abp1 form complexes that move along filaments, accumulating at regions of overlap, and driving compaction from the binding energy.

RESULTS

Srv2/CAP, enhanced by Abp1, promotes actin filament bundling and coalescence

To investigate the potential effects of Srv2/CAP and Abp1 in spatially regulating actin filaments *in vitro*, we performed visual assays using TIRF microscopy. Labeled actin filaments were polymerized in a buffer containing a crowding agent (3% dextran) to push filaments against the coverslip surface and thus maintain their positions while allowing the exchange of solutions. Once filaments were polymerized, free actin monomers were washed out and replaced with proteins of interest or a control buffer (t = 0 s), and the effects on filament organization were monitored. Despite some variability in the appearance of filaments in different fields of view at time 0, neither control buffer nor 1 μM Abp1 caused any obvious time-dependent changes in filament organization (Figure 1A). However, 1 μM Srv2/CAP alone led to crosslinking of filaments over time (Figure 1A). These effects were enhanced when 1 μM Abp1 and 1 μM Srv2/CAP were combined, inducing rapid coalescence of actin filaments into a network of thick, interconnected bundles (Figure 1A; Video S1).

To quantify the observed compaction of the filaments, we assigned the network dispersion index as the area covered by filaments in the observed region with the index at t = 0 s normalized to 1. The sharp drop in dispersion index indicates a reorganization of actin filaments into bundles (Figure 1B). The rate of remodeling, defined as the inverse of the time required to reach half-maximum compaction, was dependent on the concentration of Abp1 and Srv2/CAP (1:1 molar ratio) in the reactions and reached a maximum at ~300 nM Abp1 and Srv2/CAP (Figure 1C). Similarly, the mouse homologs of Abp1 and Srv2/CAP, together but not alone, promoted this effect, suggesting that the activity is conserved (Figure S1A). We measured the thickness of the actin filaments/bundles in our reactions by line scan analysis, comparing the fluorescence intensity at time 0 (before flowing in Srv2 + Abp1), time 1.5 min (relatively early in compaction), and time 10 min (when compaction is complete). Filaments became progressively thicker with time, reaching a maximal bundle thickness of ~5–6 filaments thick (Figure 1D), possibly limited by the hexameric oligomerization state of Srv2.

To our knowledge, such an activity of actin filaments dynamically sliding along each other to form an interconnected network of bundles (which we refer to as "coalescence") has not been reported for other actin crosslinking proteins. However, it may be related to the recently reported *in vitro* effects of anillin, which organizes actin filaments into rings and generates contractile forces that drive ring constriction[54] (see discussion).

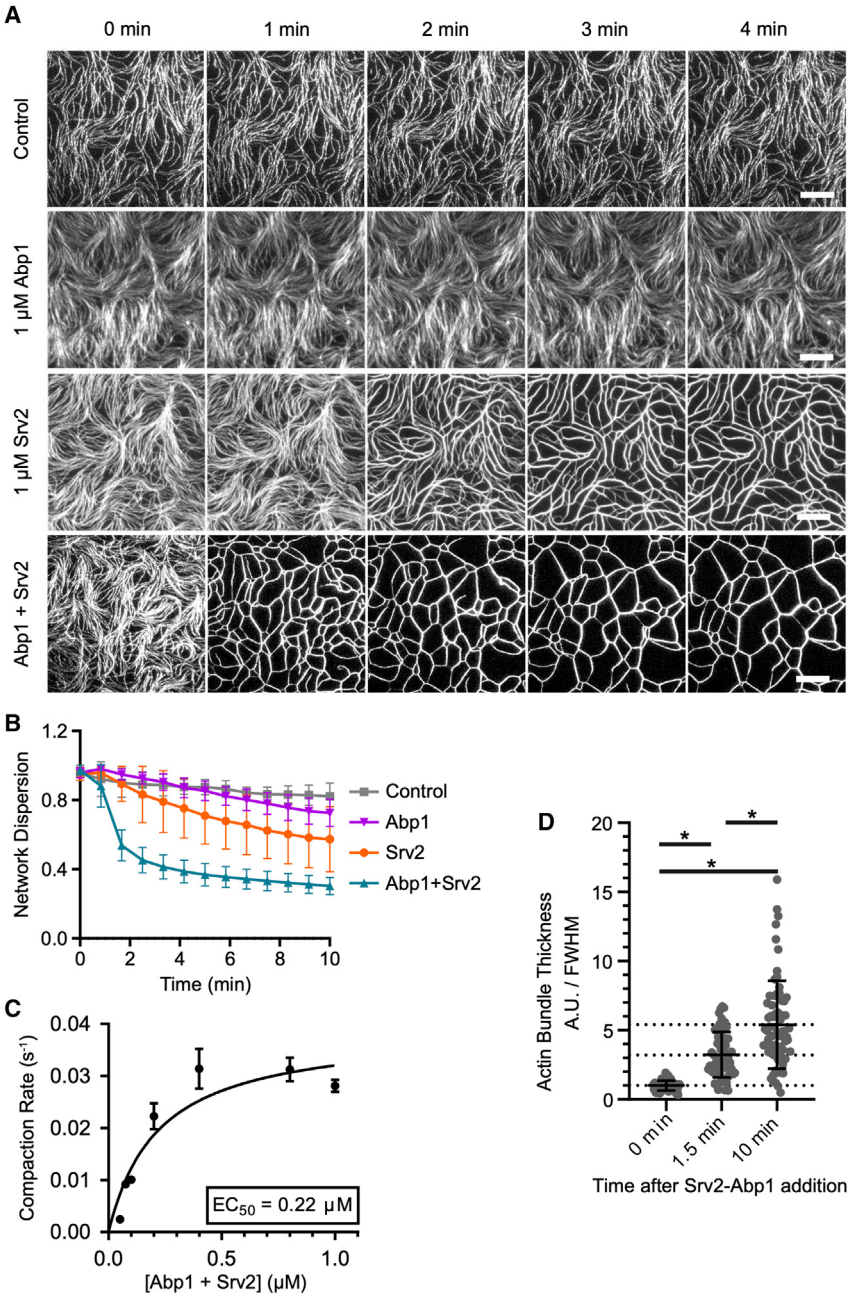

Figure 1. Srv2/CAP and Srv2/CAP-Abp1 drive the coalescence of actin filaments into bundles

(A) Time points from TIRF microscopy coalescence assays. Filaments assembled from 1 μM actin (10% OG-labeled) were exposed to 1 μM Abp1 and/or 1 μM Srv2, and the organization of filaments was monitored for 10 min, acquiring images at 10-s intervals. Scale bars, 15 μm.

(B) Quantification of the coalescence state of filaments from reactions as in (A). Network dispersion is defined as the mean area covered by filaments at a given time, divided by the initial actin-covered area. Plot shows mean (±SEM) from 10 fields of view (FOVs) in each of 3 replicates.

(C) Concentration-dependent effects of Abp1 and Srv2 (at equal molar ratio) on coalescence/compaction. Compaction rate is the inverse of time to half-minimal network dispersion. Compaction rate was plotted against Abp1 + Srv2 concentration, and points were fitted with a hyperbola, with EC_{50} defined as the concentration of Abp1 + Srv2 that yielded half-maximal compaction rate. Plot shows mean (±SEM) from 3 FOVs for each concentration.

(D) Bundle thickness assessed at different time points in reactions by measuring fluorescence intensity at full-width half-maximum (FWHM) of line segments drawn perpendicular to the bundle. Plot shows data from three independent replicates with mean (±SD) highlighted (n = 60 per condition). Fluorescence intensity values at 1.5 and 10 min were normalized to the 0 min time point (before Abp1 and Srv2 were introduced). One-way ANOVA with a Kruskal-Wallis comparisons test was used to determine statistical significance of differences between the three conditions (*p < 0.05). Additional data related to this panel are found in Figure S1 and Videos S1 and S2.

Although the Abp1-Srv2/CAP remodeling activity we observe is highly dynamic, it does not depend on ATP hydrolysis (Figure S1B). This suggests that the free energy released when filaments overlap and pack closely together may be sufficient to drive this process, as previously suggested for specific microtubule crosslinkers and for anillin in crosslinking actin filaments.[54,55] Because Srv2/CAP is also an actin-monomer-binding and recycling protein, we tested whether the presence of G-actin might affect remodeling, but no change was observed (Figure S1C). Further, we asked whether Abp1 and Srv2/CAP can crosslink filaments in a low-speed pelleting assay.[56] This experiment also shows that the bundling activity does not depend on crowding agents because, unlike the TIRF assays, the low-speed pelleting assays were performed without dextran. In the low-speed pelleting assays, Abp1 and Srv2/CAP together promoted bundling in a concentration-dependent manner, as indicated by a shift in F-actin from the supernatant to the pellet (Figure 2A). These effects were observed using both vertebrate muscle actin and *S. cerevisiae* actin (Figure 2B).

As mentioned above, Srv2/CAP and Abp1 both localize to endocytic actin patches in yeast and lamellipodial networks in mammalian cells, structures that are assembled by the branched nucleator Arp2/3 complex. Therefore, we also asked whether Srv2/CAP and Abp1 are capable of remodeling branched actin networks. Using yeast Arp2/3 complex and a Las17 VCA construct, we polymerized branched F-actin networks with differentially labeled mother filaments (magenta) and daughter filaments (cyan). We then washed out free proteins and introduced Srv2/CAP and Abp1, which led to rapid transformation of the branched networks into bundles that coalesced (Video S2). Thus, Srv2/CAP and Abp1 are capable of remodeling either branched or unbranched networks.

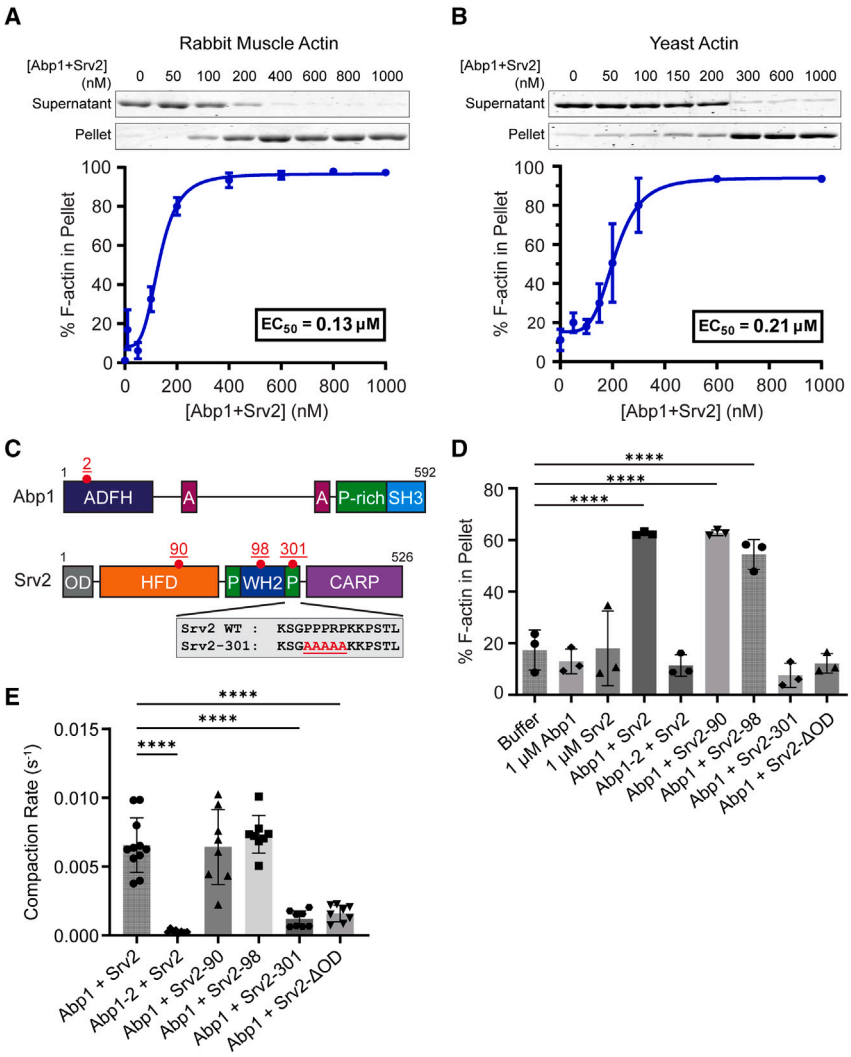

Figure 2. Domain requirements for F-actin bundling and coalescence by Srv2-Abp1

(A) Abp1 and Srv2 together bundle filaments polymerized from rabbit muscle actin in a concentration-dependent manner, as measured in low-speed pelleting assays. Representative gels show actin in the supernatant and pellet fractions (expanded images of gels showing all bands in Figure S4A). Plots show the mean percentage of F-actin in the pellet at varying Abp1 + Srv2 concentrations. Data were fit to a four-parameter dose-response curve; EC_{50} is the concentration of Abp1 + Srv2 that results in half-maximal F-actin pelleting. Plot shows mean (±SD) from 3 replicates.

(B) Same as (A) but using filaments polymerized from yeast actin (expanded images of gels showing all bands in Figure S4B). Plot shows mean (±SD) from 3 replicates.

Additional data related to (A) and (B) are in Figure S4.

(C) Schematic of Abp1 and Srv2 domains, highlighting key mutations used in each protein (red numbering): *Abp1-2*,[38] *Srv2-90*,[23] *Srv2-98*,[30] and *Srv2-301* (this study), which alters 5 residues in the P2 region of Srv2 (as indicated).

(D) Actin bundling activities for wild-type and mutant Abp1 and Srv2 proteins (1 μM each) measured in low-speed pelleting assays. Plot shows mean (±SD) from 3 replicates. Kruskal-Wallis test with multiple comparisons test used to determine the statistical significance of differences between conditions (****$p < 0.0001$).

(E) Compaction rates (quantified as in Figure 1B) for wild-type and mutant Abp1 or Srv2 proteins (0.3 μM each) in TIRF reactions. Plot shows mean (±SEM) from 8 FOVs. Representative time series for each reaction shown in Figure S2. Ordinary one-way ANOVA test with Dunnett's multiple comparisons test used to determine the statistical significance of differences between wild-type and mutant proteins (****$p < 0.0001$). Additional data related to this panel are found in Figures S2–S4.

Molecular interactions required for F-actin coalescence induced by Srv2/CAP-Abp1

To better understand the molecular requirements for the remodeling activity, we employed a set of previously characterized mutations in Abp1 and Srv2/CAP that disrupt their interactions, either with actin or each other (Figure 2C). Mutants disrupting the Abp1-F-actin interaction (*Abp1-2*) and the Abp1-Srv2/CAP interaction (*Srv2-301*) impaired Srv2/CAP-Abp1 remodeling activity (Figures 2D, 2E, and S2A). In contrast, Srv2/CAP-Abp1 remodeling activity was not altered by a mutation in the HFD domain of Srv2/CAP (*Srv2-90*), which abolishes Srv2 effects on filament severing and depolymerization, or by a mutation in the WH2 domain (*Srv2-98*), which abolishes effects on actin monomer recycling. These data suggest that Srv2/CAP-Abp1 remodeling activity depends on Srv2/CAP oligomerization, Srv2/CAP interactions with Abp1, and Abp1 interactions with F-actin.

Interestingly, a higher concentration of *Srv2-301* could support remodeling in combination with Abp1 (Figure S2B), suggesting that the *Srv2-301* mutation (which disrupts the polyproline P2 site) only partially impairs Srv2/CAP interactions with Abp1 and that other parts of Srv2/CAP may contribute to Abp1 binding. In support of this view, a higher concentration of the N-terminal half of Srv2/CAP (N-Srv2), which forms hexamers but lacks the P2 site, could support remodeling in combination with Abp1 (Figure S2B). This may also explain why mammalian CAP1, which lacks a well-defined SH3-binding P2 motif, nonetheless promotes remodeling with mammalian Abp1.

Deletion of the OD domain (*Srv2-ΔOD*), which mediates Srv2/CAP oligomerization, almost abolished remodeling (Figure S2A), with network compaction being minimal compared with full-length hexameric Srv2 (Figure 2E). The *Srv2-ΔOD* polypeptide is a dimer[23] due to dimerization of the C-terminal CARP domain,[29,57] which could facilitate a residual low level of bundling when combined with Abp1.

Taken together, these results suggest that enhanced remodeling activity by Srv2/CAP-Abp1 depends on (1) Srv2/CAP's ability to oligomerize in its N terminus, (2) Srv2/CAP's ability to bind Abp1, and (3) Abp1's ability to bind F-actin. Thus, Srv2/CAP hexamers may serve as a molecular platform/hub that alone is sufficient to remodel actin networks but is enhanced by the recruitment of Abp1 molecules with ADF-H domains that bind F-actin.

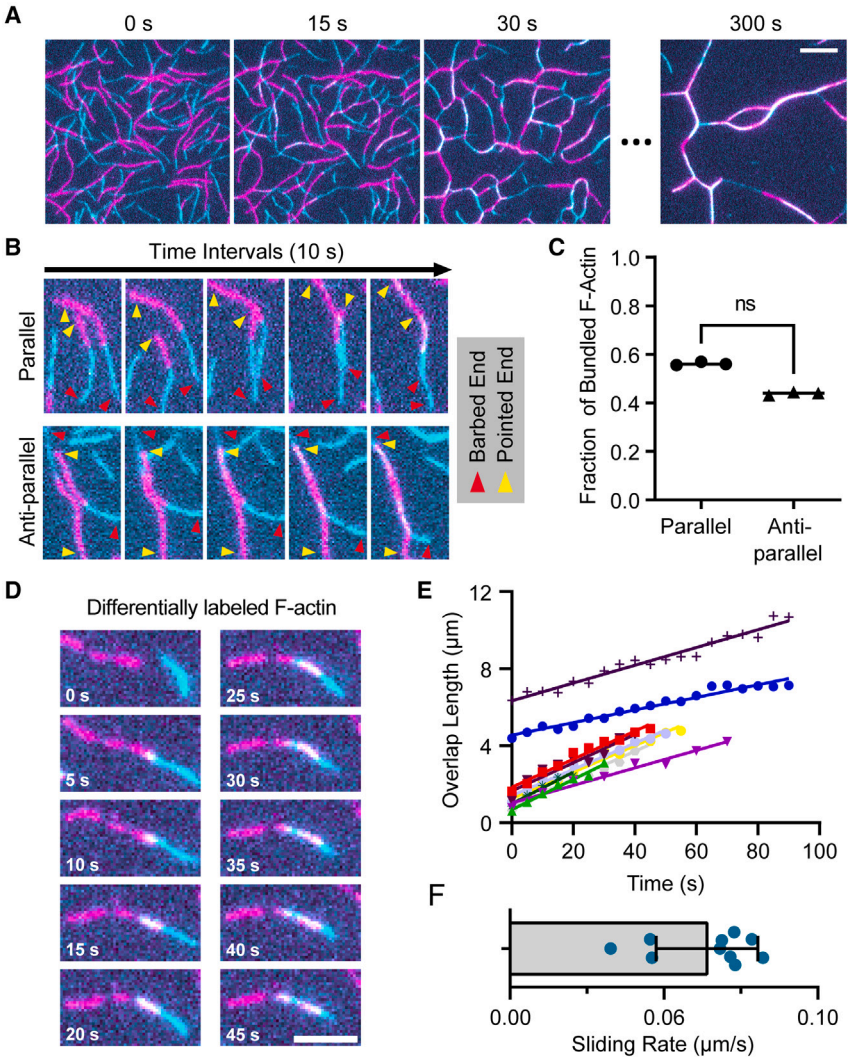

Figure 3. Srv2-Abp1 slides parallel or anti-parallel actin filament pairs to maximize filament overlap

(A) Representative TIRF microscopy assays with Abp1 and Srv2 containing polarity-marked actin filaments. Filaments were assembled initially from G-actin labeled in one color (10% DY649-actin, magenta), then further polymerized using G-actin in another color (10% OG-actin, cyan), generating filaments with cyan barbed ends and magenta pointed ends. Filaments were then exposed to 1 μM Abp1 and Srv2. Scale bars, 15 μm.

(B) Polarity of actin filament pairs (from reactions as in A) brought together by Srv2 and Abp1 was determined by tracking the filament barbed ends (red arrows) and pointed ends (yellow arrows) during bundling.

(C) Fraction of actin filament pairs bundled by Srv2-Abp1 (as in B) that are parallel and anti-parallel. Graph shows values from 3 replicates; lines indicate the means of the replicates (n = 150 filament pairs per condition).

(D) Example time-lapse imaging of two actin filaments, one labeled with 10% DY649-actin (magenta) and one with 10% OG-actin (cyan), sliding along each other in the presence of 1 μM Abp1 and Srv2. Scale bars, 5 μm.

(E) Filaments in a pair slide along each other in the direction that increases their overlap. Graph shows 10 examples, each of which exhibits increasing filament overlap with time. Measurements ended when the shorter of the two filaments fully overlaps with the longer. Lines show linear fits.

(F) Rates of filament sliding, calculated from the slopes of the lines in (E). Plot shows mean (±SD). Additional data related to this panel are found in Video S3.

Srv2/CAP alone has reduced F-actin coalescence activity (compared with Srv2/CAP-Abp1) and distinct domain requirements

Our observations in Figure 1B show that F-actin compaction by Srv2 alone (no Abp1) is slower than for Srv2-Abp1. We therefore tested whether higher concentrations of Srv2 alone (1 and 3 μM) might be able to support faster compaction. Our results show that even a 10-fold-higher concentration of Srv2 alone (3 μM) has lower activity than 0.3 μM Srv2 + 0.3 μM Abp1 (Figure S3A). Additionally, we assessed the molecular interactions required for coalescence by Srv2/CAP alone. For these experiments, we compared the activities of 1 μM Srv2 (wild type), Srv2-ΔOD, Srv2-90, Srv2-98, and N-Srv2 (each in the absence of Abp1) (Figure S3B). Our data show that oligomerization of Srv2 (disrupted by Srv2ΔOD) is required for the activity of Srv2/CAP alone, as it was for Srv2/CAP-Abp1. Further, the HFD domain (disrupted by Srv2-90) is not required for the activity of Srv2/CAP alone, as was the case for Srv2/CAP-Abp1. However, the C-terminal WH2 domain of Srv2/CAP (disrupted by Srv2-98) is required for coalescence by Srv2/CAP alone, whereas it was not required for coalescence by Srv2/CAP-Abp1. This is presumably because the interactions of Srv2/CAP hexamers with Abp1 molecules (which bind F-actin) compensate for loss of the WH2 domain. In support of this idea, N-Srv2 alone (which lacks the WH2 domain) failed to promote coalescence in the absence of Abp1.

Srv2/CAP and Abp1 bundle and slide parallel and anti-parallel actin filaments

To determine whether Abp1 and Srv2/CAP bundle actin filaments preferably into parallel or anti-parallel arrangements, we generated filaments labeled at opposite ends with two different fluorophores. This was accomplished by polymerization, first with DY647-actin (10% labeled) and then with Oregon Green (OG)-actin (10% labeled) (Figure 3A, magenta and cyan, respectively), resulting in filaments enriched in OG-actin (cyan) at their barbed ends and DY647-actin (magenta) at their pointed ends. Next, we flowed in Srv2/CAP and Abp1 and followed the polarities of the mixed-color filaments as they were organized into bundles (Figure 3B; Video S3). Quantification of these effects showed that Srv2/CAP and Abp1 organize filaments into both

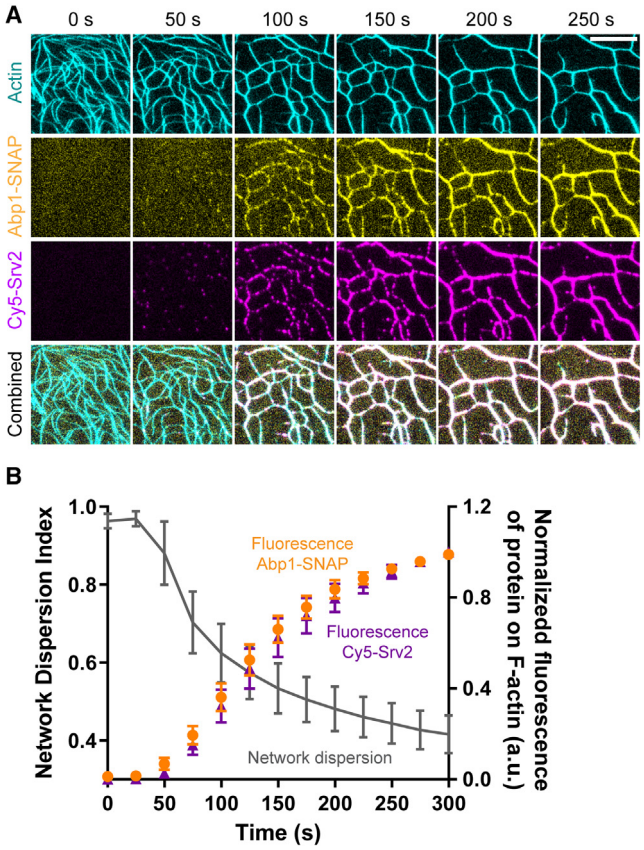

Figure 4. Abp1 and Srv2 accumulate on actin filament bundles in parallel with network compaction

(A) Time points from TIRF microscopy imaging of a reaction in which 0.3 μM Abp1 (with 10 nM Abp1-SNAP-549) and Srv2 (with 10 nM Cy5-Srv2) were flowed into a reaction chamber containing 1 μM pre-assembled actin filaments (10% OG-actin). Scale bars, 15 μm.

(B) Fluorescence intensity of Abp1-SNAP-549 and Cy5-Srv2 on F-actin over time (right axis), overlaid with actin network dispersion over time (left axis). Fluorescence values were normalized to the maximum fluorescence reached by 300 s. Plots show mean (±SEM) from 3 replicates.

parallel and anti-parallel arrangements, with only a slight preference for assembling parallel bundles (Figure 3C).

In the assays above, filaments also appeared to slide past each other, increasing their overlap as they formed bundles. To directly test for sliding, we assembled two distinct sets of filaments, differentially labeled with DY647-actin or OG-actin, but with their barbed ends capped by capping protein to prevent filament annealing. In reactions containing this mixture of the two types of labeled filaments, the addition of Srv2/CAP and Abp1 led to filaments sliding past each other (Figure 3D). The overlap between pairs of differently labeled filaments steadily increased at a rate of 0.07 μm/s, never decreasing (Figures 3E and 3F). This experiment confirms that filaments slide relative to one another. In addition, these observations reveal that the rate of sliding is fairly constant over time, even as filament overlap progressively increases. This has important implications for the mechanism by which Srv2/CAP and Abp1 dynamically crosslink filaments and drive their overlap (see discussion). This mechanism appears to be distinct from bundling induced by crosslinkers like fascin, which zipper filaments together only by forming new filament-filament interactions.[58] In contrast, filament coalescence by Srv2-Abp1 (Figure 3B) also involves the sliding of filaments, which necessitates repeatedly breaking and reforming filament-filament interactions.

Accumulation of Srv2/CAP and Abp1 on actin filaments correlates with their coalescence

To gain deeper insights into how Srv2/CAP and Abp1 drive actin filament coalescence, we generated fluorescently labeled Cy5-Srv2 and Abp1-SNAP-549 and imaged them on OG-labeled actin filaments using three-color TIRF microscopy. Pre-assembled OG-actin filaments were exposed to unlabeled Abp1 and Srv2 (0.3 μM each) spiked with low concentrations (10 nM) of Abp1-SNAP-549 and Cy5-Srv2 molecules to allow visualization of Abp1 and Srv2 within the filament networks. During filament bundling and compaction, Abp1-SNAP-549 and Cy5-Srv2 fluorescence appeared on the bundles (Figure 4A). Quantification revealed an accumulation of Abp1-SNAP-549 and Cy5-Srv2 on filaments that temporally correlated with network compaction (Figure 4B), supporting the view that the binding of Abp1 and Srv2/CAP promotes filament reorganization.

Abp1 and Srv2/CAP enhance each other's binding to actin filaments

Abp1 alone binds to the sides of actin filaments with K_D = 0.5–1.0 μM,[38] and the interaction is transient, with an average dwell time of less than 1 s.[59] Srv2/CAP binds to the sides of F-actin with K_D in the 1–10 μM range,[17] raising the possibility that its interactions with filament sides are also transient. We next compared the accumulation of Abp1-SNAP-549 on filaments in the presence and absence of unlabeled Srv2 (Figures 5A and 5B). In the presence of Srv2, there was a striking accumulation of Abp1-SNAP-549 on filaments, as opposed to little accumulation in the absence of Srv2. Conversely, we compared Cy5-Srv2 decoration of filaments in the presence and absence of unlabeled Abp1 (Figures 5C and 5D). Cy5-Srv2 accumulation on filaments was clear in the presence of Abp1 but not in its absence. Together, these observations suggest that Abp1 and Srv2/CAP form complexes that promote the interaction of the two proteins with actin filaments.

Dynamics of Srv2/CAP and Abp1 foci on actin filaments during remodeling

To gain additional insights into the dynamic behavior of Srv2-Abp1 complexes on filaments, we performed experiments at reduced concentrations of labeled Srv2 and/or Abp1. In reactions containing 5 nM Cy5-Srv2 and unlabeled Abp1 (500 nM), we observed foci of Srv2 moving along filaments (Figures 6A and 6B). The mean-squared displacement was linear in time (Figure 6C), consistent with a diffusive random walk. When we monitored reactions containing low concentrations of both proteins (5 nM Cy5-Srv2 and 100 nM Abp1-SNAP-549), we again observed foci consisting of both proteins (Figure 6D). Further, the foci remained on filaments as they underwent remodeling. Together, these observations support a model in which Srv2/CAP and Abp1 form multivalent complexes, capable of shifting position on filaments while remaining attached, and allowing filament sliding and coalescence (Figure 6E).

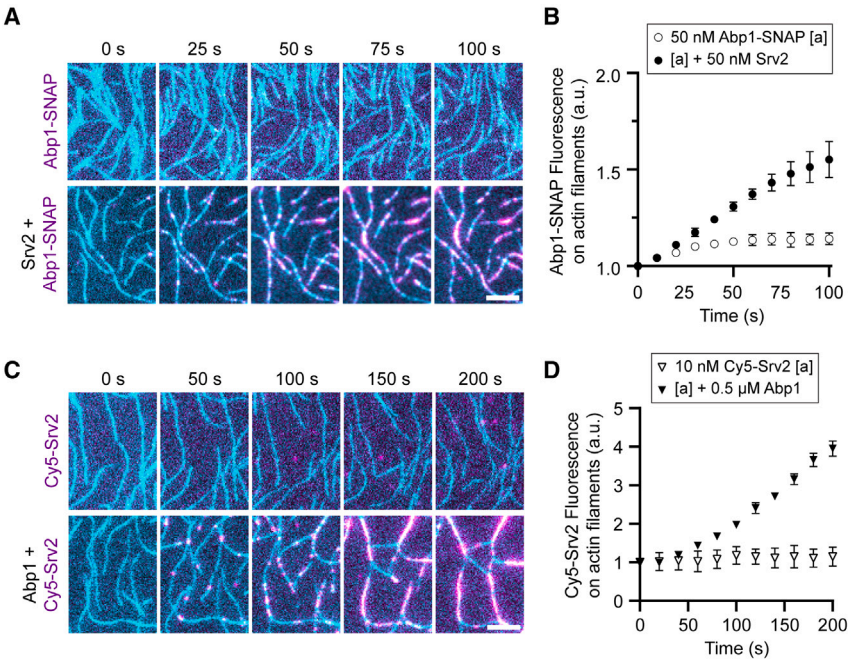

Figure 5. Abp1 and Srv2 stabilize each other's associations with actin filament bundles

(A) Unlabeled Srv2 enhances Abp1-SNAP-649 binding to actin filament bundles. Pre-assembled actin filaments (10% OG-actin, cyan) were mixed with 50 nM Abp1-SNAP-649 (magenta), with or without 50 nM unlabeled Srv2. Scale bars, 5 μm.

(B) Integrated fluorescence intensity of Abp1-SNAP-649 over time (in the FOV) as observed in (A). Plots show mean (±SD) from 2 replicates.

(C) Unlabeled Abp1 enhances Cy5-Srv2 binding to actin filament bundles. Pre-assembled actin filaments (10% OG-actin, cyan) were mixed with 10 nM labeled Srv2 (Cy5-Srv2, magenta), with or without 500 nM unlabeled Abp1. Lower panel shows the indicated region at higher time resolution (1-s intervals), highlighting an event where Cy5-Srv2 molecules contact two adjacent actin filaments, which then become bundled. Scale bars, 5 μm.

(D) Integrated fluorescence intensity of Cy5-Srv2 over time (in the FOV) as observed in (C). Plots show mean (±SD) from 2 replicates.

In vivo evidence for Srv2/CAP remodeling of actin architecture

The remodeling activity of Srv2/CAP prompted us to investigate its importance for actin organization *in vivo*. *S. cerevisiae* Srv2/CAP and Abp1 localize to cortical actin patches, and loss of Srv2/CAP (and to a lesser extent Abp1) alters the initial assembly phase, inward movement phase, and lifetime of actin patches.[32,60,61] Further, specific mutations in Srv2/CAP's HFD, WH2, and CARP domains each compromise patch dynamics,[32] suggesting that Srv2/CAP's functions in F-actin disassembly and monomer recycling are important for normal cortical actin patch dynamics. In addition, Srv2/CAP is required for proper actin cable formation, as *srv2Δ* cells exhibit thinner, shorter, and more disorganized cables.[16,23,32,62] In contrast, we and others have shown that *abp1Δ* alone causes no visible defects in cellular actin organization.[38,46] This inspired us to consider whether the remodeling activity of Srv2/CAP contributes to cable formation.

To assess actin cable architecture, we imaged fixed, Alexa 488-phalloidin-stained yeast cells using structured illumination microscopy (SIM) (Figure 7A). As previously reported, *srv2Δ* resulted in enlarged cells (Figure 7B), with depolarized actin patches and thinner, shorter, and disorganized actin cables (upper row, Figure 7A). In addition, we treated cells with CK666, which inhibits Arp2/3-mediated actin assembly and removes actin patches, prior to fixation (lower row, Figure 7A). This treatment also liberates the actin pool normally tied up in actin patches, making it available for formin-dependent cable assembly,[63] allowing a more direct assessment of mutant cable phenotypes (without potential indirect effects from altered patch dynamics reducing the monomer pool). Indeed, we found that CK666 treatment restored normal cable organization to *srv2-98* cells (a mutation that disrupts the WH2 domain), suggesting that the primary defect in *srv2-98* mutants may be slow patch turnover, which indirectly alters cables. On the other hand, after CK666 treatment, *srv2Δ*, *srv2-90*, and *srv2-ΔOD* each exhibited varying degrees of disorganized cables, marked by a significant increase relative to wild type in cable segment number (Figure 7C). However, *srv2-301*, which weakens binding of the P2 domain to Abp1, showed mostly wild-type cable organization, suggesting that Abp1-Srv2/CAP interactions are not critical for cable architecture *in vivo*, e.g., if Srv2/CAP functions without Abp1 in cable organization. This is further supported by the observation that *abp1Δ* cells have wild-type cable organization. Regardless, *srv2-ΔOD* mutation caused a striking cable phenotype, consistent with its biochemical effects in remodeling, suggesting that Srv2/CAP's remodeling activity may contribute to maintaining proper cable architecture *in vivo*.

Finally, we reinvestigated the long-standing genetic observation that *abp1Δ* and *srv2*Δ mutations show synthetic growth defects in combination with a deletion of fimbrin/Sac6 (*sac6Δ*).[45–47] We reasoned that if Sac6 and Srv2/CAP-Abp1 share functions in F-actin remodeling, then a mutation that disrupts Srv2/CAP-Abp1 interactions (*srv2-301*) might show synthetic defects in the *sac6Δ* background. To address this, we crossed *srv2-301* and *sac6Δ* strains and compared the resulting single and double mutants for cellular F-actin organization, morphology, and growth at 25°C and 35°C (Figures 7E and 7F). Our results show that *sac6Δ* partially compromises cell growth and partially depolarizes actin patches, as previously reported,[49] and *srv2-301* cells are indistinguishable from wild type, as expected (because *abp1Δ* is indistinguishable from wild type). However, *sac6Δ srv2-301* double mutants are more defective than *sac6Δ* single mutants in cell size (enlargement) and cell growth. Thus, loss of Srv2/CAP-Abp1 interactions (*srv2-301*) exacerbates cell growth and morphology in the *sac6Δ* background, consistent with Srv2/CAP-Abp1 performing a role in cellular F-actin remodeling, which is redundant with fimbrin/Sac6.

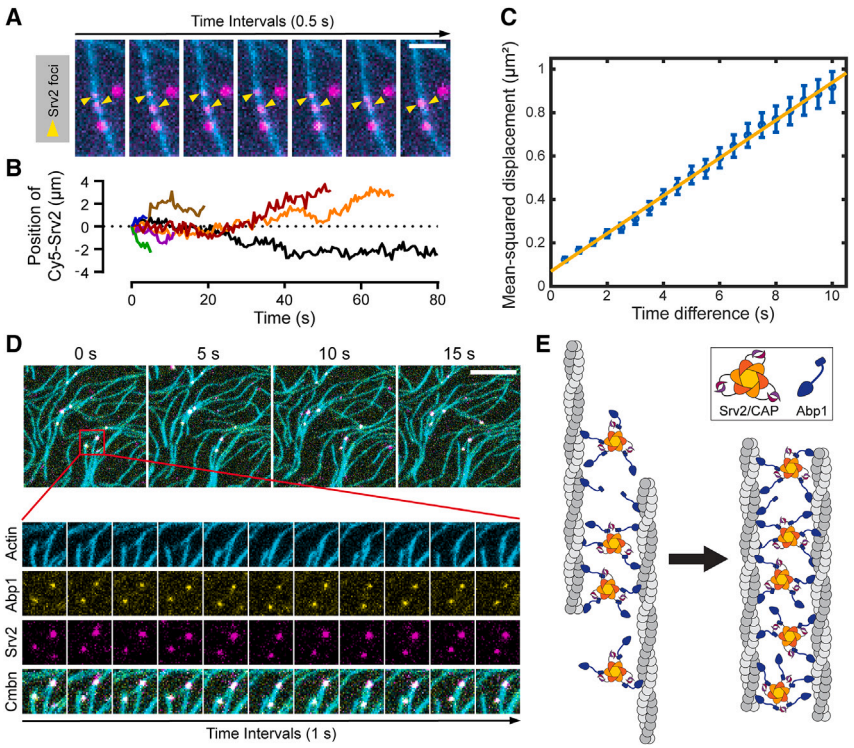

Figure 6. Dynamics of Abp1-Srv2 foci on actin filaments

(A) Time series images of labeled Srv2 foci on individual actin filaments in the presence of unlabeled Abp1. Pre-assembled actin filaments (10% OG-actin, cyan) were mixed with 5 nM Cy5-Srv2 (magenta), with or without 500 nM unlabeled Abp1. Two spots of Cy5-Srv2 (yellow arrows) diffuse on a filament. Scale bars, 3 μm.

(B) Eight example time-position records of Cy5-Srv2 foci moving along actin filaments.

(C) Position records in (B) were aggregated to compute the mean-squared distance moved (circles; ±SEM) over time intervals of 0.5–10 s. Agreement with unweighted linear fit (line) indicates movement is diffusive.

(D) Colocalizaton of Abp1-SNAP-549 and Cy5-Srv2 in foci on actin filaments (1 μM, 10% OG-labeled). Reactions contain 100 nM Abp1-SNAP-549 and 10 nM Cy5-Srv2. Magnified area shows that Abp1-SNAP-549 and Cy5-Srv2 remain colocalized in foci as filaments are dynamically rearranged. Scale bars, 10 μm.

(E) Working model for Abp1 and Srv2/CAP interacting with actin filament sides and driving filament bundling and coalescence (see discussion). Over time, the overlap between filaments increases and Srv2/CAP-Abp1 complexes accumulate in the overlap zone.

DISCUSSION

Our observations suggest a new role for Srv2/CAP, enhanced by its association with Abp1, in driving an unusual form of actin filament bundling, sliding, and coalescence. The novel filament sliding and coalescence may be related to the oligomeric architecture of Srv2/CAP, which forms a six-bladed hub that dynamically interacts with various members of the ADF-H family of proteins. Previous work has shown that, in concert with ADF-H proteins cofilin and twinfilin, Srv2/CAP accelerates depolymerization of actin filaments from their ends.[25,27,28] However, interactions of Srv2/CAP with the ADF-H protein Abp1 have long remained puzzling. Our results here suggest that Srv2/CAP and Abp1 interact to drive actin filament rearrangements via bundling, sliding, and coalescence.

The effects of Srv2/CAP (and Abp1) in sliding filaments along each other, and the resulting coalescence, are distinct from those of most other actin crosslinking/bundling proteins (e.g., fascin, α-actinin, and fimbrin), which cause filament bundling but not sliding or compaction. However, they may bear some relationship to the recently reported activities of anillin.[54] Similar to anillin, Srv2/CAP and Abp1 together slide on filaments and promote parallel and anti-parallel filament sliding that leads to increasing overlap, independent of an external supply of energy. Further, both anillin and Srv2/CAP-Abp1 drive the formation of networks, or circles, of highly curved filament bundles. This suggests that both crosslinkers can perform work against the flexible rigidity of actin filaments. On the other hand, with anillin, the velocity of filament sliding decreases as the filament overlap zone increases, whereas, with Srv2/CAP-Abp1, the sliding velocity remains constant as the overlap zone increases (Figure 3E). This difference could be due to anillin promoting filament sliding and overlap by a purely entropically driven mechanism.[55,64] In contrast, Srv2/CAP-Abp1 may drive filament overlap by accumulating in the overlap region as sliding progresses, steadily increasing the number of energetically favorable binding interactions (Srv2/CAP-Abp1 to F-actin). The multi-valent hexameric architecture of Srv2/CAP, combined with the highly dynamic nature of Abp1 molecules interacting with Srv2/CAP via their SH3 domains, and interacting with F-actin via their ADF-H domains,[59] may ensure that the increasing number of Srv2/CAP-Abp1 crosslinks does not significantly slow filament sliding as overlap increases.

Our results suggest that Srv2/CAP plays a more central role in the remodeling process compared with Abp1. Furthermore, they offer an explanation for why Abp1 and Srv2/CAP interact *in vivo*, possibly accounting for the long-standing genetic observation that mutations in *S. cerevisiae* Abp1 and Srv2/CAP are each synthetic lethal with mutations in the F-actin bundler Sac6/Fimbrin.[45–47] Recent cryoelectron tomographic studies reveal that endocytic actin networks assembled by the branched nucleator (Arp2/3 complex) contain a surprisingly high fraction of unbranched filaments, and many of the unbranched filaments at these sites are organized into bundles or are bent.[11,12] Modeling and theory studies suggest that elastic energy stored in bent filaments might be released at specific steps of endocytosis to provide additional force to drive vesicle invagination.[10,65,66] The remodeling activities of Srv2/CAP (and Abp1) may contribute to rearrangements in F-actin architecture at endocytic sites, helping transform branched regions of networks into bundles. Consistent with this possibility, Srv2/CAP and Abp1 localize to sites of endocytosis, and genetic loss of either

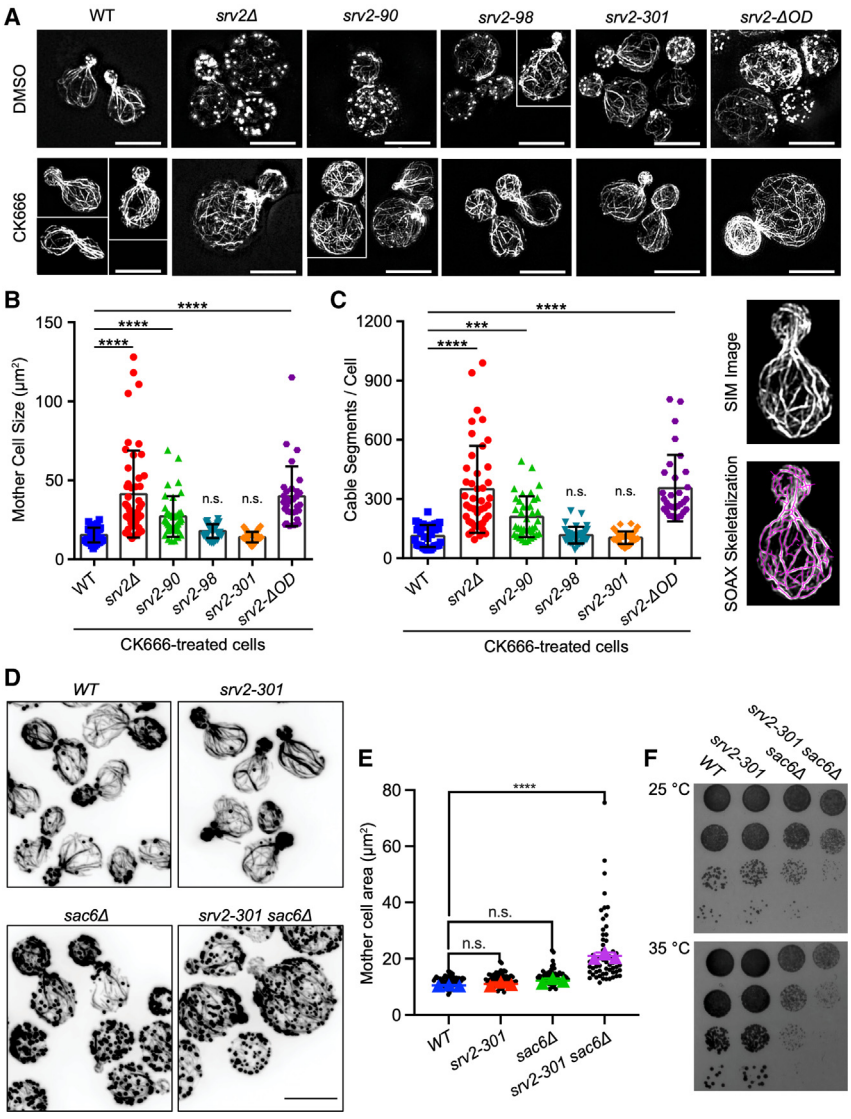

Figure 7. *In vivo* evidence for Srv2 and Srv2-Abp1 remodeling of yeast actin networks

(A) Representative structured illumination microscopy (SIM) of F-actin organization (Alexa 488-phalloidin staining) in fixed wild-type, *srv2Δ*, *srv2-90*, *srv2-98*, *srv2-301*, and *srv2-ΔOD* cells, treated with DMSO (control) or 100 μM CK666. Scale bars, 5 μm.

(B) Average mother cell size (area of two-dimensional projection) of CK666-treated, fixed cells from SIM, quantified for n > 30 cells per strain (wild type, n = 37; *srv2Δ*, n = 49; *srv2-90*, n = 39; *srv2-98*, n = 33; *srv2-301*, n = 43; *srv2-ΔOD*, n = 31). Error bars, SD. ****p ≤ 0.0001; n.s. p > 0.05 by one-way ANOVA with Kruskal-Wallis test.

(C) Average number of cable segments per cell quantified from SIM images of CK666-treated, fixed cells by automated SOAX program for n > 30 cells per strain (wild type, n = 36; *srv2Δ*, n = 43; *srv2-90*, n = 39; *srv2-98*, n = 34; *srv2-301*, n = 35; *srv2-ΔOD*, n = 31). Error bars, SD. Right insets show representative SIM image of one CK666-treated, fixed wild-type cell with SOAX-skeletonized actin cables. Error bars, SD. ****p ≤ 0.0001, ***p ≤ 0.001; n.s. p > 0.05 by one-way ANOVA with Kruskal-Wallis test.

(D) Representative cell images of indicated yeast strains fixed and stained with Alexa 488-phalloidin. Images are maximum intensity projections. Scale bars, 5 μm.

(E) Mother cell sizes (dots) measured for the same strains as in (D). Data from three replicates. Larger symbols (color) represent the mean of each replicate. Error bars, SD. ****p < 0.0001; n.s. p > 0.05 by one-way ANOVA using Dunnett's multiple comparison test.

(F) Cell growth assays comparing 10-fold serial dilutions of the same yeast strains as in (D) and (E), grown for 2 days on YPD plates at the indicated temperatures.

Srv2/CAP or Abp1 leads to defects in endocytosis in both yeast and mammalian cells.[32–35,67–69] Importantly, *srv2Δ* phenotypes are more severe than those of *abp1Δ* in yeast, which may stem from Srv2 having a more central role in remodeling compared with Abp1.

Could the bundling/coalescence activities of Srv2/CAP play a role in yeast actin cable formation? We found that *srv2ΔOD* cells have striking defects in cable architecture, characterized by a loss of longer cables and the appearance of numerous short cables or cable fragments (Figure 7). Similar defects have been described for *srv2Δ* cells[16,30,32]; however, until now, this cable phenotype has been difficult to reconcile with the known activities of Srv2/CAP in promoting actin depolymerization[25,27,28] because loss of depolymerization effects should in principle lead to longer rather than shorter cables. Each cable is a parallel bundle, comprising multiple, overlapping shorter filaments.[70] Our results raise the intriguing possibility that Srv2's bundling and coalescence activity helps hold together the shorter (overlapping) filament segments in cables and that loss of the bundling activity leads to the shorter cable fragments seen in *srv2Δ* and *srv2ΔOD* cells. The lack of obvious cable defects in *abp1Δ* mutants[36–38] is consistent with Srv2/CAP playing the central role in filament bundling and coalescence. Thus, Srv2/CAP and Abp1 may function together at cortical actin patches to remodel actin networks, while Srv2/CAP functions alone in cable formation without the assistance of Abp1. This proposed role for Srv2/CAP-Abp1 interactions being important for F-actin remodeling at actin patches is supported by the genetic interactions we observed between *srv2-301* and *sac6Δ*.

We observed that both the yeast and mammalian homologs of Abp1 and Srv2/CAP promote F-actin coalescence, suggesting that this interacting pair of proteins may play an important role in organizing actin networks across a broad range of eukaryotic species. Consistent with this idea, Abp1 and CAP colocalize at the leading edge of motile mammalian cells and in sarcomeric structures in *C. elegans* muscle, and both proteins are required for the proper organization of metazoan actin networks *in vivo* and normal rates of endocytosis.[20,34,35,71,72] Although the sequence of the P2 motif in mammalian CAP diverges from the P2 motif of yeast Srv2/CAP, we found that mutating the P2 motif in yeast Srv2/CAP only weakened, but did not eliminate, its

remodeling activities with Abp1. Further, at higher concentrations, the hexameric N-Srv2 polypeptide, consisting of the OD and HFD domains (but lacking P1, WH2, P2, and CARP domains), was able to promote remodeling in combination with Abp1. Thus, other domains in yeast and mammalian Srv2/CAP may contribute to the Abp1-Srv2/CAP interactions that drive coalescence.

In the future, it will be important to determine how the actin filament remodeling activities of Abp1 and Srv2/CAP are integrated with Srv2/CAP's other known functions in promoting actin turnover. For example, Abp1 facilitates the recruitment of Srv2/CAP to F-actin structures *in vivo*, which could enhance Srv2/CAP's effects with cofilin and twinfilin in promoting F-actin disassembly. On the other hand, when bundled filaments are decorated by Srv2/CAP-Abp1 complexes, the ADF-H domains of Abp1 could dampen the severing and depolymerization effects of cofilin and twinfilin, given that the ADF-H domains of Abp1 and cofilin are structurally similar and bind to overlapping sites on F-actin.[38] Ultimately, understanding how this complex set of proteins works in concert to coordinate actin remodeling and turnover may require the development of new *in vitro* assays that simultaneously monitor changes in actin filament spatial organization, severing, and depolymerization.

STAR★METHODS

Detailed methods are provided in the online version of this paper and include the following:

- KEY RESOURCES TABLE
- RESOURCE AVAILABILITY
  - Lead contact
  - Materials availability
  - Data and code availability
- EXPERIMENTAL MODEL AND SUBJECT DETAILS
- METHOD DETAILS
  - Plasmid Construction
  - Protein Expression and Purification
  - Total Internal Reflection Fluorescence (TIRF) Microscopy
  - Actin Filament Bundling Assays
  - Cell Imaging and Analysis
- QUANTIFICATION AND STATISTICAL ANALYSIS

SUPPLEMENTAL INFORMATION

Supplemental information can be found online at https://doi.org/10.1016/j.cub.2023.09.032.

ACKNOWLEDGMENTS

We are grateful to Omar Quintero-Monzon for early observations of actin bundling by Abp1 and Srv2, Emil Reisler (UCLA) for generously providing the *S. cerevisiae* actin used in Figure 2, and David Drubin for providing a plasmid for expressing mAbp1. This work was supported by grants from NIGMS (R35 GM134895 to B.L.G. and R01 GM81648 to J.G.) and the Brandeis NSF MRSEC, Bioinspired Soft Materials (DMR-2011486).

AUTHOR CONTRIBUTIONS

Conceptualization, writing manuscript, and review and editing of manuscript, S.G., J.G., G.J.H., J.O.M., and B.L.G.; project administration, supervision, and resources, J.G. and B.L.G.; data curation, investigation, methodology, visualization, and validation, S.G., G.J.H., and J.O.M.; formal analysis, S.G., G.J.H., J.O.M., and J.G.

DECLARATION OF INTERESTS

The authors declare no competing interests.

Received: January 17, 2023
Revised: July 20, 2023
Accepted: September 13, 2023
Published: October 4, 2023

REFERENCES

1. Rotty, J.D., Wu, C., and Bear, J.E. (2013). New insights into the regulation and cellular functions of the ARP2/3 complex. Nat. Rev. Mol. Cell Biol. *14*, 7–12. https://doi.org/10.1038/nrm3492.
2. Goode, B.L., Eskin, J.A., and Wendland, B. (2015). Actin and endocytosis in budding yeast. Genetics *199*, 315–358. https://doi.org/10.1534/genetics.112.145540.
3. Campellone, K.G., and Welch, M.D. (2010). A nucleator arms race: cellular control of actin assembly. Nat. Rev. Mol. Cell Biol. *11*, 237–251. https://doi.org/10.1038/nrm2867.
4. Welch, M.D., and Mullins, R.D. (2002). Cellular control of actin nucleation. Annu. Rev. Cell Dev. Biol. *18*, 247–288. https://doi.org/10.1146/annurev.cellbio.18.040202.112133.
5. Stevenson, R.P., Veltman, D., and Machesky, L.M. (2012). Actin-bundling proteins in cancer progression at a glance. J. Cell Sci. *125*, 1073–1079. https://doi.org/10.1242/jcs.093799.
6. Li, T.D., Bieling, P., Weichsel, J., Mullins, R.D., and Fletcher, D.A. (2022). The molecular mechanism of load adaptation by branched actin networks. eLife *11*, e73145. https://doi.org/10.7554/eLife.73145.
7. Ydenberg, C.A., Padrick, S.B., Sweeney, M.O., Gandhi, M., Sokolova, O., and Goode, B.L. (2013). GMF severs actin-Arp2/3 complex branch junctions by a Cofilin-like mechanism. Curr. Biol. *23*, 1037–1045. https://doi.org/10.1016/j.cub.2013.04.058.
8. Hotulainen, P., and Lappalainen, P. (2006). Stress fibers are generated by two distinct actin assembly mechanisms in motile cells. J. Cell Biol. *173*, 383–394. https://doi.org/10.1083/jcb.200511093.
9. Murugesan, S., Hong, J., Yi, J., Li, D., Beach, J.R., Shao, L., Meinhardt, J., Madison, G., Wu, X., Betzig, E., et al. (2016). Formin-generated actomyosin arcs propel T cell receptor microcluster movement at the immune synapse. J. Cell Biol. *215*, 383–399. https://doi.org/10.1083/jcb.201603080.
10. Akamatsu, M., Vasan, R., Serwas, D., Ferrin, M.A., Rangamani, P., and Drubin, D.G. (2020). Principles of self-organization and load adaptation by the actin cytoskeleton during clathrin-mediated endocytosis. eLife *9*, e49840. https://doi.org/10.7554/eLife.49840.
11. Jin, M., Shirazinejad, C., Wang, B., Yan, A., Schöneberg, J., Upadhyayula, S., Xu, K., and Drubin, D.G. (2022). Branched actin networks are organized for asymmetric force production during clathrin-mediated endocytosis in mammalian cells. Nat. Commun. *13*, 3578. https://doi.org/10.1038/s41467-022-31207-5.
12. Serwas, D., Akamatsu, M., Moayed, A., Vegesna, K., Vasan, R., Hill, J.M., Schöneberg, J., Davies, K.M., Rangamani, P., and Drubin, D.G. (2022). Mechanistic insights into actin force generation during vesicle formation from cryo-electron tomography. Dev. Cell *57*, 1132–1145.e5. https://doi.org/10.1016/j.devcel.2022.04.012.

13. Fedor-Chaiken, M., Deschenes, R.J., and Broach, J.R. (1990). SRV2, a gene required for RAS activation of adenylate cyclase in yeast. Cell *61*, 329–340. https://doi.org/10.1016/0092-8674(90)90813-t.

14. Field, J., Vojtek, A., Ballester, R., Bolger, G., Colicelli, J., Ferguson, K., Gerst, J., Kataoka, T., Michaeli, T., Powers, S., et al. (1990). Cloning and characterization of CAP, the S. cerevisiae gene encoding the 70 kd adenylyl cyclase-associated protein. Cell *61*, 319–327. https://doi.org/10.1016/0092-8674(90)90812-S.

15. Ono, S. (2013). The role of cyclase-associated protein in regulating actin filament dynamics - more than a monomer-sequestration factor. J. Cell Sci. *126*, 3249–3258. https://doi.org/10.1242/jcs.128231.

16. Chaudhry, F., Breitsprecher, D., Little, K., Sharov, G., Sokolova, O., and Goode, B.L. (2013). Srv2/cyclase-associated protein forms hexameric shurikens that directly catalyze actin filament severing by cofilin. Mol. Biol. Cell *24*, 31–41. https://doi.org/10.1091/mbc.E12-08-0589.

17. Jansen, S., Collins, A., Golden, L., Sokolova, O., and Goode, B.L. (2014). Structure and mechanism of mouse cyclase-associated protein (CAP1) in regulating actin dynamics. J. Biol. Chem. *289*, 30732–30742. https://doi.org/10.1074/jbc.M114.601765.

18. Purde, V., Busch, F., Kudryashova, E., Wysocki, V.H., and Kudryashov, D.S. (2019). Oligomerization affects the ability of human cyclase-associated proteins 1 and 2 to promote actin severing by cofilins. Int. J. Mol. Sci. *20*, 5647. https://doi.org/10.3390/ijms20225647.

19. Kodera, N., Abe, H., Nguyen, P.D.N., and Ono, S. (2021). Native cyclase-associated protein and actin from Xenopus laevis oocytes form a unique 4:4 complex with a tripartite structure. J. Biol. Chem. *296*, 100649. https://doi.org/10.1016/j.jbc.2021.100649.

20. Moriyama, K., and Yahara, I. (2002). Human CAP1 is a key factor in the recycling of cofilin and actin for rapid actin turnover. J. Cell Sci. *115*, 1591–1601.

21. Balcer, H.I., Goodman, A.L., Rodal, A.A., Smith, E., Kugler, J., Heuser, J.E., and Goode, B.L. (2003). Coordinated regulation of actin filament turnover by a high-molecular-weight Srv2/CAP complex, Cofilin, Profilin, and Aip1. Curr. Biol. *13*, 2159–2169. https://doi.org/10.1016/j.cub.2003.11.051.

22. Mattila, P.K., Quintero-Monzon, O., Kugler, J., Moseley, J.B., Almo, S.C., Lappalainen, P., and Goode, B.L. (2004). A high-affinity interaction with ADP-actin monomers underlies the mechanism and in vivo function of Srv2/cyclase-associated protein. Mol. Biol. Cell *15*, 5158–5171. https://doi.org/10.1091/mbc.e04-06-0444.

23. Quintero-Monzon, O., Jonasson, E.M., Bertling, E., Talarico, L., Chaudhry, F., Sihvo, M., Lappalainen, P., and Goode, B.L. (2009). Reconstitution and dissection of the 600-kDa Srv2/CAP complex: roles for oligomerization and cofilin-actin binding in driving actin turnover. J. Biol. Chem. *284*, 10923–10934. https://doi.org/10.1074/jbc.M808760200.

24. Kotila, T., Kogan, K., Enkavi, G., Guo, S., Vattulainen, I., Goode, B.L., and Lappalainen, P. (2018). Structural basis of actin monomer re-charging by cyclase-associated protein. Nat. Commun. *9*, 1892. https://doi.org/10.1038/s41467-018-04231-7.

25. Johnston, A.B., Collins, A., and Goode, B.L. (2015). High-speed depolymerization at actin filament ends jointly catalysed by Twinfilin and Srv2/CAP. Nat. Cell Biol. *17*, 1504–1511. https://doi.org/10.1038/ncb3252.

26. Hilton, D.M., Aguilar, R.M., Johnston, A.B., and Goode, B.L. (2018). Species-specific functions of twinfilin in actin filament depolymerization. J. Mol. Biol. *430*, 3323–3336. https://doi.org/10.1016/j.jmb.2018.06.025.

27. Kotila, T., Wioland, H., Enkavi, G., Kogan, K., Vattulainen, I., Jégou, A., Romet-Lemonne, G., and Lappalainen, P. (2019). Mechanism of synergistic actin filament pointed end depolymerization by cyclase-associated protein and cofilin. Nat. Commun. *10*, 5320. https://doi.org/10.1038/s41467-019-13213-2.

28. Shekhar, S., Chung, J., Kondev, J., Gelles, J., and Goode, B.L. (2019). Synergy between cyclase-associated protein and cofilin accelerates actin filament depolymerization by two orders of magnitude. Nat. Commun. *10*, 5319. https://doi.org/10.1038/s41467-019-13268-1.

29. Dodatko, T., Fedorov, A.A., Grynberg, M., Patskovsky, Y., Rozwarski, D.A., Jaroszewski, L., Aronoff-Spencer, E., Kondraskina, E., Irving, T., Godzik, A., et al. (2004). Crystal structure of the actin binding domain of the cyclase-associated protein. Biochemistry *43*, 10628–10641. https://doi.org/10.1021/bi049071r.

30. Chaudhry, F., Little, K., Talarico, L., Quintero-Monzon, O., and Goode, B.L. (2010). A central role for the WH2 domain of Srv2/CAP in recharging actin monomers to drive actin turnover in vitro and in vivo. Cytoskeleton (Hoboken) *67*, 120–133. https://doi.org/10.1002/cm.20429.

31. Chaudhry, F., Jansen, S., Little, K., Suarez, C., Boujemaa-Paterski, R., Blanchoin, L., and Goode, B.L. (2014). Autonomous and in trans functions for the two halves of Srv2/CAP in promoting actin turnover. Cytoskeleton (Hoboken) *71*, 351–360. https://doi.org/10.1002/cm.21170.

32. Toshima, J.Y., Horikomi, C., Okada, A., Hatori, M.N., Nagano, M., Masuda, A., Yamamoto, W., Siekhaus, D.E., and Toshima, J. (2016). Srv2/CAP is required for polarized actin cable assembly and patch internalization during clathrin-mediated endocytosis. J. Cell Sci. *129*, 367–379. https://doi.org/10.1242/jcs.176651.

33. Peche, V.S., Holak, T.A., Burgute, B.D., Kosmas, K., Kale, S.P., Wunderlich, F.T., Elhamine, F., Stehle, R., Pfitzer, G., Nohroudi, K., et al. (2013). Ablation of cyclase-associated protein 2 (CAP2) leads to cardiomyopathy. Cell. Mol. Life Sci. *70*, 527–543. https://doi.org/10.1007/s00018-012-1142-y.

34. Nomura, K., Ono, K., and Ono, S. (2012). CAS-1, a C. elegans cyclase-associated protein, is required for sarcomeric actin assembly in striated muscle. J. Cell Sci. *125*, 4077–4089. https://doi.org/10.1242/jcs.104950.

35. Bertling, E., Hotulainen, P., Mattila, P.K., Matilainen, T., Salminen, M., and Lappalainen, P. (2004). Cyclase-associated protein 1 (CAP1) promotes cofilin-induced actin dynamics in mammalian nonmuscle cells. Mol. Biol. Cell *15*, 2324–2334. https://doi.org/10.1091/mbc.e04-01-0048.

36. Drubin, D.G., Miller, K.G., and Botstein, D. (1988). Yeast actin-binding proteins: evidence for a role in morphogenesis. J. Cell Biol. *107*, 2551–2561. https://doi.org/10.1083/jcb.107.6.2551.

37. Goode, B.L., Rodal, A.A., Barnes, G., and Drubin, D.G. (2001). Activation of the Arp2/3 complex by the actin filament binding protein Abp1p. J. Cell Biol. *153*, 627–634.

38. Quintero-Monzon, O., Rodal, A.A., Strokopytov, B., Almo, S.C., and Goode, B.L. (2005). Structural and functional dissection of the Abp1 ADFH actin-binding domain reveals versatile in vivo adapter functions. Mol. Biol. Cell *16*, 3128–3139. https://doi.org/10.1091/mbc.E05-01-0059.

39. Poukkula, M., Kremneva, E., Serlachius, M., and Lappalainen, P. (2011). Actin-depolymerizing factor homology domain: a conserved fold performing diverse roles in cytoskeletal dynamics. Cytoskeleton (Hoboken) *68*, 471–490. https://doi.org/10.1002/cm.20530.

40. Fazi, B., Cope, M.J.T.V., Douangamath, A., Ferracuti, S., Schirwitz, K., Zucconi, A., Drubin, D.G., Wilmanns, M., Cesareni, G., and Castagnoli, L. (2002). Unusual binding properties of the SH3 domain of the yeast actin-binding protein Abp1: structural and functional analysis. J. Biol. Chem. *277*, 5290–5298. https://doi.org/10.1074/jbc.M109848200.

41. Garcia, B., Stollar, E.J., and Davidson, A.R. (2012). The importance of conserved features of yeast actin-binding protein 1 (Abp1p): the conditional nature of essentiality. Genetics *191*, 1199–1211. https://doi.org/10.1534/genetics.112.141739.

42. Stollar, E.J., Garcia, B., Chong, P.A., Rath, A., Lin, H., Forman-Kay, J.D., and Davidson, A.R. (2009). Structural, functional, and bioinformatic studies demonstrate the crucial role of an extended peptide binding site for the SH3 domain of yeast Abp1p. J. Biol. Chem. *284*, 26918–26927. https://doi.org/10.1074/jbc.M109.028431.

43. Landgraf, C., Panni, S., Montecchi-Palazzi, L., Castagnoli, L., Schneider-Mergener, J., Volkmer-Engert, R., and Cesareni, G. (2004). Protein interaction networks by proteome peptide scanning. PLoS Biol. *2*, E14. https://doi.org/10.1371/journal.pbio.0020014.

44. Freeman, N.L., Lila, T.O.M., Mintzer, K.A., Chen, Z., Pahk, A.J., Ren, R., Drubin, D.G., and Field, J. (1996). A conserved proline-rich region of the Saccharomyces cerevisiae cyclase-associated protein binds SH3

domains and modulates cytoskeletal localization. Mol. Cell. Biol. *16*, 548–556.

45. Adams, A.E., Cooper, J.A., and Drubin, D.G. (1993). Unexpected combinations of null mutations in genes encoding the actin cytoskeleton are lethal in yeast. Mol. Biol. Cell *4*, 459–468. https://doi.org/10.1091/mbc.4.5.459.

46. Holtzman, D., Yang, S., and Drubin, D. (1993). Synthetic-lethal interactions identify two novel genes, SLA1 and SLA2, that control membrane cytoskeleton assembly in Saccharomyces cerevisiae. J. Cell Biol. *122*, 635–644. https://doi.org/10.1083/jcb.122.3.635.

47. Lila, T., and Drubin, D.G. (1997). Evidence for physical and functional interactions among two Saccharomyces cerevisiae SH3 domain proteins, an adenylyl cyclase-associated protein and the actin cytoskeleton. Mol. Biol. Cell *8*, 367–385.

48. Glenney, J.R., Kaulfus, P., Matsudaira, P., and Weber, K. (1981). F-actin binding and bundling properties of fimbrin, a major cytoskeletal protein of microvillus core filaments. J. Biol. Chem. *256*, 9283–9288.

49. Adams, A.E.M., Botstein, D., and Drubin, D.G. (1991). Requirement of yeast fimbrin for actin organization and morphogenesis in vivo. Nature *354*, 404–408. https://doi.org/10.1038/354404a0.

50. Höfer, D., Ness, W., and Drenckhahn, D. (1997). Sorting of actin isoforms in chicken auditory hair cells. J. Cell Sci. *110*, 765–770. https://doi.org/10.1242/jcs.110.6.765.

51. Goodman, A., Goode, B.L., Matsudaira, P., and Fink, G.R. (2003). The Saccharomyces cerevisiae calponin/transgelin homolog Scp1 functions with fimbrin to regulate stability and organization of the actin cytoskeleton. Mol. Biol. Cell *14*, 2617–2629. https://doi.org/10.1091/mbc.e03-01-0028.

52. Miao, Y., Han, X., Zheng, L., Xie, Y., Mu, Y., Yates, J.R., and Drubin, D.G. (2016). Fimbrin phosphorylation by metaphase Cdk1 regulates actin cable dynamics in budding yeast. Nat. Commun. *7*, 11265. https://doi.org/10.1038/ncomms11265.

53. Watanabe, M., Watanabe, D., Nogami, S., Morishita, S., and Ohya, Y. (2009). Comprehensive and quantitative analysis of yeast deletion mutants defective in apical and isotropic bud growth. Curr. Genet. *55*, 365–380. https://doi.org/10.1007/s00294-009-0251-0.

54. Kučera, O., Siahaan, V., Janda, D., Dijkstra, S.H., Pilátová, E., Zatecka, E., Diez, S., Braun, M., and Lansky, Z. (2021). Anillin propels myosin-independent constriction of actin rings. Nat. Commun. *12*, 4595. https://doi.org/10.1038/s41467-021-24474-1.

55. Lansky, Z., Braun, M., Lüdecke, A., Schlierf, M., ten Wolde, P.R., Janson, M.E., and Diez, S. (2015). Diffusible crosslinkers generate directed forces in microtubule networks. Cell *160*, 1159–1168. https://doi.org/10.1016/j.cell.2015.01.051.

56. Maekawa, S., Endo, S., and Sakai, H. (1983). Purification and partial characterization of a new protein in porcine brain which bundles actin filaments. J. Biochem. *94*, 1329–1337.

57. Ksiazek, D., Brandstetter, H., Israel, L., Bourenkov, G.P., Katchalova, G., Janssen, K.-P., Bartunik, H.D., Noegel, A.A., Schleicher, M., and Holak, T.A. (2003). Structure of the N-terminal domain of the adenylyl cyclase-associated protein (CAP) from Dictyostelium discoideum. Structure *11*, 1171–1178. https://doi.org/10.1016/S0969-2126(03)00180-1.

58. Breitsprecher, D., Koestler, S.A., Chizhov, I., Nemethova, M., Mueller, J., Goode, B.L., Small, J.V., Rottner, K., and Faix, J. (2011). Cofilin cooperates with fascin to disassemble filopodial actin filaments. J. Cell Sci. *124*, 3305–3318. https://doi.org/10.1242/jcs.086934.

59. Guo, S., Sokolova, O.S., Chung, J., Padrick, S., Gelles, J., and Goode, B.L. (2018). Abp1 promotes Arp2/3 complex-dependent actin nucleation and stabilizes branch junctions by antagonizing GMF. Nat. Commun. *9*, 2895. https://doi.org/10.1038/s41467-018-05260-y.

60. Kaksonen, M., Sun, Y., and Drubin, D.G. (2003). A pathway for association of receptors, adaptors, and actin during endocytic internalization. Cell *115*, 475–487. https://doi.org/10.1016/S0092-8674(03)00883-3.

61. Galletta, B.J., Chuang, D.Y., and Cooper, J.A. (2008). Distinct roles for Arp2/3 regulators in actin assembly and endocytosis. PLoS Biol. *6*, e1. https://doi.org/10.1371/journal.pbio.0060001.

62. Gao, L., and Bretscher, A. (2008). Analysis of unregulated formin activity reveals how yeast can balance F-actin assembly between different microfilament-based organizations. Mol. Biol. Cell *19*, 1474–1484. https://doi.org/10.1091/mbc.e07-05-0520.

63. Suarez, C., Carroll, R.T., Burke, T.A., Christensen, J.R., Bestul, A.J., Sees, J.A., James, M.L., Sirotkin, V., and Kovar, D.R. (2015). Profilin regulates F-actin network homeostasis by favoring formin over Arp2/3 complex. Dev. Cell *32*, 43–53. https://doi.org/10.1016/j.devcel.2014.10.027.

64. Braun, M., Lansky, Z., Hilitski, F., Dogic, Z., and Diez, S. (2016). Entropic forces drive contraction of cytoskeletal networks. BioEssays *38*, 474–481. https://doi.org/10.1002/bies.201500183.

65. Lacy, M.M., Ma, R., Ravindra, N.G., and Berro, J. (2018). Molecular mechanisms of force production in clathrin-mediated endocytosis. FEBS Lett. *592*, 3586–3605. https://doi.org/10.1002/1873-3468.13192.

66. Ma, R., and Berro, J. (2019). Crosslinking actin networks produces compressive force. Cytoskeleton (Hoboken) *76*, 346–354. https://doi.org/10.1002/cm.21552.

67. Burston, H.E., Maldonado-Báez, L., Davey, M., Montpetit, B., Schluter, C., Wendland, B., and Conibear, E. (2009). Regulators of yeast endocytosis identified by systematic quantitative analysis. J. Cell Biol. *185*, 1097–1110. https://doi.org/10.1083/jcb.200811116.

68. Aghamohammadzadeh, S., Smaczynska-de Rooij, I.I., and Ayscough, K.R. (2014). An Abp1-dependent route of endocytosis functions when the classical endocytic pathway in yeast is inhibited. PLoS One *9*, e103311. https://doi.org/10.1371/journal.pone.0103311.

69. Hummel, D.R., and Kaksonen, M. (2022). Spatio-temporal regulation of endocytic protein assembly by SH3 domains in yeast. Mol. Biol. Cell *34*, ar19. https://doi.org/10.1091/mbc.e22-09-0406.

70. Moseley, J.B., Okada, K., Balcer, H.I., Kovar, D.R., Pollard, T.D., and Goode, B.L. (2006). Twinfilin is an actin-filament-severing protein and promotes rapid turnover of actin structures in vivo. J. Cell Sci. *119*, 1547–1557. https://doi.org/10.1242/jcs.02860.

71. Kessels, M.M., Engqvist-Goldstein, A.E., and Drubin, D.G. (2000). Association of mouse actin-binding protein 1 (mAbp1/SH3P7), an Src kinase target, with dynamic regions of the cortical actin cytoskeleton in response to Rac1 activation. Mol. Biol. Cell *11*, 393–412. https://doi.org/10.1091/mbc.11.1.393.

72. Butkevich, E., Bodensiek, K., Fakhri, N., von Roden, K., Schaap, I.A.T., Majoul, I., Schmidt, C.F., and Klopfenstein, D.R. (2015). Drebrin-like protein DBN-1 is a sarcomere component that stabilizes actin filaments during muscle contraction. Nat. Commun. *6*, 7523. https://doi.org/10.1038/ncomms8523.

73. Xu, T., Vavylonis, D., Tsai, F.C., Koenderink, G.H., Nie, W., Yusuf, E., Lee, I.J., Wu, J.Q., and Huang, X. (2015). SOAX: a software for quantification of 3D biopolymer networks. Sci. Rep. *5*, 9081. https://doi.org/10.1038/srep09081.

74. Schindelin, J., Arganda-Carreras, I., Frise, E., Kaynig, V., Longair, M., Pietzsch, T., Preibisch, S., Rueden, C., Saalfeld, S., Schmid, B., et al. (2012). Fiji: an open-source platform for biological-image analysis. Nat. Methods *9*, 676–682. https://doi.org/10.1038/nmeth.2019.

STAR★METHODS

KEY RESOURCES TABLE

REAGENT or RESOURCE	SOURCE	IDENTIFIER
Bacterial and virus strains		
BL21 (DE3) pLysS Competent Cells	Promega	L1195
Rosetta 2(DE3) Competent Cells (pRARE plasmid)	Millipore Sigma	71397-4
Biological samples		
Actin from rabbit hind-leg muscle	Pel-Freez	RMA
S. cerevisiae Arp2/3 complex	Guo et al.[59]	N/A
S. cerevisiae Actin	Emil Reisler	Emil Reisler-US
Chemicals, peptides, and recombinant proteins		
Dextran from Leuconostoc spp. with Mr 450,000-650,000, pH 7.4	Millipore Sigma	31392-10G
mPEG-silane, MW 2,000	Laysan Bio	MPEG-SIL-2000-5g
Biotin-PEG-silane, MW 3,400	Laysan Bio	Biotin-PEG-SIL-3400-500mg
Oregon Green 488 iodoacetamide	ThermoFisher	O6010D (discontinued)
NHS-X-Biotin	Sigma-Aldrich	03189-50MG
PreScission Protease	GE LifeScience/Cytiva	27084301
DY-649-Maleimide	Dyomics	649-03
SNAP-Surface 549	New England Biolab	S9112S
Cy5 Maleimide Mono-Reactive Dye	GE LifeScience/Cytiva	PA25031
Alexa Fluor 488 Phalloidin	ThermoFisher	A12379
VECTASHIELD Antifade Mounting Media	Vector Laboratories	H-1000-10
CK-666	Sigma-Aldrich	SML0006-5MG
GST-VCA (Las17) protein	Ydenberg et al.[7]	Bruce Goode
Mouse CAP1 protein	Jansen et al.[17]	Bruce Goode
Yeast Abp1 protein	This Paper	Bruce Goode
Yeast Abp1-2 protein	This Paper	Bruce Goode
Yeast Abp1-SNAP-549 protein	This Paper	Bruce Goode
Mouse Abp1 protein	This Paper	Bruce Goode
Yeast Srv2 protein	This Paper	Bruce Goode
Yeast Srv2-90 protein	This Paper	Bruce Goode
Yeast Srv2-98 protein	This Paper	Bruce Goode
Yeast Srv2-301 protein	This Paper	Bruce Goode
Yeast Srv2-ΔOD protein	This Paper	Bruce Goode
Yeast Srv2-Cy5 protein	This Paper	Bruce Goode
Experimental models: Organisms/strains		
MATα lys2-801(oc) hisΔ200 ura3-52 leu2-3, 112 trp1-1(am)	Bruce Goode	Bruce Goode, BGY311
MATα lys2-801(oc) hisΔ200 ura3-52 leu2-3, 112 trp1-1(am), srv2Δ::HIS3	Bertling et al.[35]	Bruce Goode, BGY330
MATα lys2-801(oc) hisΔ200 ura3-52 leu2-3, 112 trp1-1(am), SRV2::TRP1	This Paper	Bruce Goode, SGY0036
MATα lys2-801(oc) hisΔ200 ura3-52 leu2-3, 112 trp1-1(am), srv2Δ50::TRP1 (srv2ΔOD)	Quintero-Monzon et al.[23]	Bruce Goode, BGY1217
MATα lys2-801(oc) hisΔ200 ura3-52 leu2-3, 112 trp1-1(am), srv2-90::TRP1	Quintero-Monzon et al.[23]	Bruce Goode, BGY1206
MATα lys2-801(oc) hisΔ200 ura3-52 leu2-3, 112 trp1-1(am), srv2-98::TRP1	Chaudhry et al.[30]	Bruce Goode, BGY4133
MATα lys2-801(oc) hisΔ200 ura3-52 leu2-3, 112 trp1-1(am), srv2-301::TRP1	This Paper	Bruce Goode, SGY0041

(*Continued on next page*)

Continued

REAGENT or RESOURCE	SOURCE	IDENTIFIER
MATa lys2-801(oc) hisΔ200 ura3-52 leu2-3, 112 trp1-1(am), sac6Δ::URA3	This Paper	Bruce Goode
Recombinant DNA		
pGEX-6P1-Abp1 (yeast)	Guo et al.[59]	Bruce Goode, pBG2175
pGEX-6P1-Abp1-2 (yeast)	This paper	Bruce Goode, pSG23
pGEX-6P1-Abp1-SNAP (yeast)	Guo et al.[59]	Bruce Goode, pBG2176
pGEX-6P1-mAbp1 (mouse)	This paper	Bruce Goode, pBG2180
pHAT2-6His-Srv2	Quintero-Monzon et al.[23]	Bruce Goode, pBG873
pHAT2-6His-Srv2-90	Quintero-Monzon et al.[23]	Bruce Goode, pBG863
pHAT2-6His-Srv2-98	Quintero-Monzon et al.[23]	Bruce Goode, pBG870
pHAT2-6His-Srv2-301	This paper	Bruce Goode, pBG2078
pHAT2-6His-Srv2-ΔOD	Quintero-Monzon et al.[23]	Bruce Goode, pBG874
pRS314-SRV2::TRP1	Quintero-Monzon et al.[23]	Bruce Goode, pBG335
pRS314-SRV2-301::TRP1	This paper	Bruce Goode, pBG2192
Software and algorithms		
NIS Elements software	Nikon Instruments	https://www.nikoninstruments.com/Products/Software; RRID: SCR_014329
Fiji / ImageJ	NIH – public domain	http://fiji.sc; RRID: SCR_002285
GraphPad Prism 10.0c	GraphPad Software	RRID: SCR_002798
SOAX	Xu et al.[73]	https://www.lehigh.edu/~div206/soax/
Other		
PierceTM Glutathione Agarose	ThermoFisher	16101
Ni-NTA Agarose	ThermoFisher	R90110
PD-10 column	GE LifeScience/Cytiva	17085101
Mono Q 5/50 GL	GE LifeScience/Cytiva	17516601
Custom μ-Slide VI 0.4 flow chambers (no coverslip included)	Ibidi	80601
120 μm double-sided tape	Grace Bio-Labs	double-sided tape

RESOURCE AVAILABILITY

Lead contact

Further information and requests for resources and reagents should be directed to and will be fulfilled by the lead contact, Bruce Goode (goode@brandeis.edu).

Materials availability

Plasmids and yeast strains generated in this study are available from the lead contact author.

Data and code availability

- All data reported in this paper will be shared by the lead contact upon request.
- This paper does not report original code.
- Any additional information required to reanalyze the data reported in this paper is available from the lead contact upon request.

EXPERIMENTAL MODEL AND SUBJECT DETAILS

For the in vivo experiments shown in Figure 7, we used wildtype and mutant *Saccharomyces cerevisiae* strains in the S288C background. Yeast strains carrying *srv2ΔOD*, *srv2-90*, and *srv2-98* mutants integrated at the endogenous *SRV2* locus, being expressed under the control of their own (*SRV2*) promoter, were generated previously.[23] The identical strategy was used here to generate a new strain expressing *srv2-301* (KSGPPPRPKKPSTL to KSGAAAAAKKPSTL). Site directed mutagenesis was performed on an *SRV2*::*TRP1* integration vector (pBG334) to produce the *srv2-301::TRP1* integration plasmid (pBG2192). Next, *SRV2::TRP1* and *srv2-301::TRP1* integration plasmids were linearized by SacII digestion and transformed into an *srv2Δ::HIS3* strain (BGY330) to create *SRV2*::*TRP1* (WT) and *srv2-301*::TRP1 strains. Separately, a *sac6Δ::URA3* strain was generated by replacing the *SAC6* coding

sequence with *URA3*. All strains were confirmed by colony PCR analysis. Potential genetic interactions between *sac6Δ::URA3 and srv2-301::TRP1* (versus *SRV2::TRP1*) were tested by crosses and tetrad analysis. For the experiments shown in Figure 7, yeast cells were grown at 25°C in liquid YEPD media until they reached log phase (OD_{600} = 0.4-0.6), then fixed and imaged as described below under method details.

METHOD DETAILS

Plasmid Construction

All materials were obtained from Sigma-Aldrich (St. Louis, MO) unless noted. Expression plasmids pGEX-Abp1 and pGEX-Abp1-SNAP were generated previously.[59] Expression plasmids in pHAT2 backbone for expressing wildtype, truncated, and mutant Srv2 constructs were generated previously.[16,23] Expression plasmid pGEX-Abp1-2 was generated by PCR amplifying mutant *S. cerevisiae* Abp1 gene from a previously generated yeast GAL overexpression plasmid[38] and sub-cloning the resulting inserts into BamHI and NotI sites of pGEX-6P1. Expression plasmid pGEX-mAbp1 was generated by PCR amplifying the mouse Abp1 coding region from the pGAT2-mAbp1 (1-433) plasmid[71] and sub-cloning the insert into BamHI and NotI sites of pGEX-6P1. The expression plasmid pHAT2-Srv2-301 was generated by site-directed mutagenesis of the wildtype expression plasmid. All constructs were verified by sequencing.

Protein Expression and Purification

Rabbit skeletal muscle actin was purified from acetone powder generated from frozen ground hind leg muscle tissue of young rabbits (PelFreez, Rogers, AR). Lyophilized acetone powder stored at -80°C was mechanically sheared in a coffee grinder, resuspended in G-buffer (5 mM Tris-HCl pH 7.5, 0.5 mM DTT, 0.2 mM ATP, 0.1 mM $CaCl_2$), and then cleared by centrifugation for 20 min at 50,000 × g. Actin was polymerized by the addition of 2 mM $MgCl_2$ and 50mM NaCl and incubated overnight at 4°C. F-actin was pelleted by centrifugation for 150 min at 361,000 × *g*, and the pellet solubilized by Dounce homogenization and dialyzed against G-buffer for 48 h at 4°C. Monomeric actin was then precleared at 435,000 × g, and loaded onto a S200 (16/60) gel filtration column (GE Healthcare, Marlborough, MA) equilibrated in G-Buffer. Fractions containing actin were stored at 4°C. For labeling actin with biotin or Oregon Green (OG), the F-actin pellet described above was homogenized and dialyzed against G-buffer lacking DTT. Monomeric actin was then polymerized by adding an equal volume of 2X labeling buffer (50 mM Imidazole pH 7.5, 200 mM KCl, 0.3 mM ATP, 4 mM $MgCl_2$). After 5 min, the actin was mixed with a 5-fold molar excess of NHS-XX-Biotin (Merck KGaA, Darmstadt, Germany), Oregon-Green-488 iodoacetamide (Invitrogen, Carlsbad, CA), or DY-649-maleimide (Dyomics, Jena, Germany) resuspended in anhydrous DMF, and incubated in the dark for 15 h at 4°C. Labeled F-actin was pelleted as above, and the pellet was rinsed briefly with G-buffer, then depolymerized by Dounce homogenization, and dialyzed against G-buffer for 48 h at 4°C. Labeled, monomeric actin was purified further on an S200 (16/60) gel filtration column as above. Aliquots of biotin-conjugated actin were snap frozen in liquid nitrogen and stored at -80°C. OG-488-actin was dialyzed for 15 h against G-buffer with 50% glycerol and stored at -20°C.

Full-length Abp1 polypeptides (GST- and GST-SNAP-tagged) were expressed and/or labeled as described previously.[59] Briefly, *E. coli* strain BL21 (DE3) pLysS carrying the plasmid were grown in TB media to OD_{600} = 1.0 at 37 °C, then protein expression was induced for 16 h at 18 °C by addition of 0.8 mM isopropyl-β-D-thiogalactopyranoside (IPTG). Cells were harvested by centrifugation and resuspended in 50 mL of 2X Phosphate-buffered saline (PBS), supplemented freshly with 1mM EDTA, 1 mM DTT, 1 mM PMSF, and a standard mixture of protease inhibitors. Cells were lysed by sonication on ice and clarified by centrifugation at 38,000 × g for 20 min. The resulting supernatant was incubated with 1 mL glutathione-agarose beads for at least 2 h at 4°C, rotating. Beads were washed five times with 2X PBS before Abp1 was released by cleavage with PreScission protease (GE Healthcare) for 16 h at 4°C. Released Abp1 was purified further on a MonoQ (5/5) anion exchange column (GE Healthcare) equilibrated in HEK buffer (20 mM Na^+-HEPES pH 7.5, 1 mM EDTA, 50 mM KCl), and eluted with a 20 column volume linear salt gradient (0-1 M KCl). Peak fractions were determined by SDS-PAGE analysis and concentrated. For purifying SNAP-tagged Abp1 (Abp1-SNAP), the same procedure was followed except the concentrated fractions from the MonoQ column were supplemented with 1 mM DTT and incubated at 25°C for 2 h with a 1-5 molar excess of SNAP-Surface dye (New England Biolab, Ipswich, MA). Labeling efficiency was determined spectrophotometrically using absorbance at 650 nm and an extinction coefficient of 250,000 $M^{-1}cm^{-1}$ for Surface 649, or absorbance at 550 nm and an extinction coefficient of 150,000 $M^{-1}cm^{-1}$ for Surface 549. Dye absorbance was combined with protein absorbance at 280 nm with an extinction coefficient of 81,360 $M^{-1}cm^{-1}$ for Abp1-SNAP to measure the labeling efficiency. The final protein product was exchanged into $HEKDG_5$ (HEK with 1mM DTT and 5% glycerol) using a PD-10 desalting column (GE Healthcare), aliquoted, snap-frozen in liquid N_2, and stored at -80 °C.

Srv2/CAP polypeptides (full-length, truncation, and mutants) were expressed in *E. coli* strain BL21 with pRARE plasmid carrying rare codons. Stains carrying the expression plasmids were grown in TB media to OD_{600} = 1.0 at 37 °C, then induced with 0.8 mM IPTG for 16 h at 18 °C. Cells were harvested by centrifugation and resuspended in 2X Phosphate-buffered saline (PBS), supplemented freshly with 1 mM EDTA, 50 mM imidazole, 1 mM PMSF, and a standard mixture of protease inhibitors. Cells were lysed by sonication on ice and clarified by centrifugation at 38,000 × g for 20 min. The resulting supernatant was incubated with 1 mL Ni-NTA beads for 1 h at 4°C, rotating. Beads were collected, washed 3 times with wash buffer (2X PBS, 1 mM EDTA, 50 mM imidazole, and 1 mM DTT), and eluted with wash buffer + 200 mM imidazole. Eluted fractions were then concentrated and exchanged into HEK buffer using a PD-10 column (GE Healthcare). For labeling full-length Srv2 polypeptide with fluorophore, the same procedure was followed except the protein-bound Ni-NTA beads were washed and eluted with wash buffer with 0.2 mM TCEP instead of 1 mM DTT. The eluted

fractions were concentrated and incubated with at least 5-fold molar excess of Cy5-maleimide dye (GE Healthcare) for 30 min at 25 °C and additionally 14 h at 4 °C. Then, excess dye was quenched with 5 mM DTT and separated from labeled protein using a PD-10 column with $HEKDG_5$ buffer. The final product was aliquoted, snap-frozen in liquid N_2, and stored at -80 °C.

Total Internal Reflection Fluorescence (TIRF) Microscopy

In all experiments, 24x60 mm coverslips (Fisher Scientific, Pittsburgh, PA) were first cleaned by sonication in detergent for 60 min, followed by successive sonication in 1M KOH and 1M HCl for 20 min each, then sonication in ethanol for 60 min. Coverslips were next washed extensively with H_2O, dried in an N_2-stream, layered with 200 μl of 80% ethanol pH 2.0, 2 mg/mL methoxy-poly(ethylene glycol)-silane M.W. 2,000 and 2 μg/mL biotin-poly(ethylene glycol)-silane M.W. 3,400 (Laysan Bio, Arab, AL), and incubated for 16 h at 70°C. Flow cells were assembled by rinsing the coated coverslips extensively with H_2O, then attaching it to a plastic flow chamber (Ibidi, Martinsried, Germany) with 2.5 cm × 2 mm × 120 μm double-sided tape (Grace Bio-Labs, Bend, OR) and epoxy resin (Devcon, Riviera Beach, FL). Before all experiments, flow cells were treated for 1 min with HBSA (HEK buffer with 1% BSA) and 1 min with 0.1 mg/mL streptavidin dissolved in HBSA. Flow cells were then equilibrated with 1x TIRF buffer (10 mM K^+-imidazole, 50 mM KCl, 1 mM $MgCl_2$, 1 mM EGTA, 0.2 mM ATP, 10 mM DTT, 15 mM glucose, 20 μg/mL catalase, 100 μg/mL glucose oxidase, and 3% dextran from Leuconostoc spp. with M_r 450,000-650,000, pH 7.4) before initiating each reaction. Solutions in TIRF chambers were exchanged using a syringe-pump (Harvard Apparatus, Holliston, MA) set at 60 μL/min flow rate. Time-lapse TIRF microscopy was performed using a Nikon-Ti200 inverted microscope (Nikon Instruments, Melville, NY) equipped with a MLC400 Monolithic Laser Combiner (Agilent Technology, Santa Clara, CA), a TIRF-objective with a numerical aperture of 1.49 (Nikon Instruments), and an EMCCD camera (Andor iXon, Belfast, Northern Ireland). The pixel size corresponded to either 0.27 μm × 0.27 μm or 0.18 μm × 0.18 μm (with 1.5 X on-scope magnification). Unless noted otherwise, all reactions were acquired using 50 ms exposure times. During recordings, focus was maintained using the Perfect Focus System (Nikon Instruments). All recorded movies were analyzed using ImageJ software within the FIJI suite.[74]

To visualize the effects of Abp1 and/or Srv2/CAP on unbranched filaments, 1 μM actin (10% OG-labeled) was polymerized in the flow chamber. Once filaments reached a desired density and length (> 10 μm), unpolymerized actin monomers were washed out using 1X TIRF buffer, and proteins of interests were introduced. Images were captured for 15 min at 10 s intervals. For studying the effects of Abp1 and Srv2/CAP on branched networks (Video S2), we first assembled unbranched filaments (10% OG-labeled) as above, and then nucleated differentially-labeled daughter branches from their sides by introducing 1 μM actin (10% DY649-labeled), 5 nM *S. cerevisiae* Arp2/3 complex, and 100 nM Las17 GST-VCA. Next, free proteins were washed out, and Abp1 and Srv2/CAP were introduced. These reactions were also used to measure the rates of sliding between differentially labeled actin filaments (Figures 3D–3F).

To measure filament dispersion, each field of view (FOV) of the recorded movies (typically 3-4 FOVs per recorded movie) was first processed by using the "background subtraction" function in ImageJ (50 pixels rolling ball radius with sliding paraboloid) and cropped to exclude out-of-focus area. A lower threshold of fluorescence signal was then established based on the first frame of each FOV movie using the "threshold" function in ImageJ, in order to exclude background areas not covered by actin filaments. Using the set lower threshold, pixel area covered by actin filaments over time was measured for each FOV movie. To compute the dispersion index, pixel area covered by actin filaments at a given time was normalized to the maximum actin covered pixel area for each FOV movie.

Bundle thickness (Figure 1D) was measured in FIJI from the TIRF images of coalescence assays at time points (0, 1.5, and 10 min) after flowing in Srv2/CAP and Abp1. The rolling ball background subtraction algorithm (ball radius, 50 pixels) was applied to images. Next, the segmented line tool was used to draw lines orthogonal to the actin filaments/bundles in the FOV. Line segments were not drawn over bundle intersections and line segments were purposely positioned to minimize nearby bundles and to avoid measurement redundancy. The intensity of the line segment was plotted and fit with a two-dimensional Gaussian in FIJI. The intensity at full-width half-max (FWHM) for each line trace was recorded at 0, 1.5, and 10 min after flowing in Srv2/CAP and Abp1. The average thickness of bundles in the presence of Srv2/CAP and Abp1 at 1.5 and 10 min was calculated by normalizing the FWHM intensity to the 0 min time point.

To determine the polarity of actin bundles generated by Abp1 and Srv2/CAP (Figures 3B and 3C), we used actin filaments differentially labeled at their two ends. 1 μM actin (10% DY649-labeled) was polymerized to approximately 3 μm in length. Then excess actin monomers were washed out using 1X TIRF buffer, and 1 μM actin (10% OG-labeled) was introduced. Filaments were elongated to > 10 μm, and then excess actin monomers were washed out using 1X TIRF buffer. The resulting filaments had barbed ends enriched in OG-actin and pointed end enriched in DY649-actin. Finally, the chamber was washed with 1X TIRF buffer, and Abp1 and Srv2/CAP were introduced.

To visualize labeled Abp1 and Srv2 during the process of actin filament bundling and coalescence, preassembled filaments (10% OG-actin) were exposed to a combination of labeled (Abp1-SNAP-549 and Cy5-Srv2) and/or unlabeled Abp1 and Srv2 in TIRF buffer. Images were recorded at 1 s intervals. To determine the diffusive behavior of labeled Srv2 complexes on actin filaments, filaments were incubated with unlabeled Abp1 and Cy5-Srv2 and recorded at 0.5 s intervals. Positions of the Cy5-Srv2 foci over time were determined with reference to one end of the filament.

Actin Filament Bundling Assays

Low-speed pelleting assays were used to determine the F-actin bundling effects of Abp1 and/or Srv2/CAP. Actin filaments were assembled from purified rabbit muscle or yeast actin in F-Buffer (20 mM Tris-HCl, pH 7.5, 50 mM KCl, 0.5 mM DTT, 0.5 mM ATP,

2 mM $MgCl_2$) for 16 hr at 4 °C. Proteins of interests were added to pre-assembled actin filaments (2 μM) in F-Buffer and incubated for 1 hr at 25 °C. Reactions were then centrifuged at low speed (20,000 × *g*) for 10 min, and the supernatants and pellets were analyzed by SDS-PAGE.

Cell Imaging and Analysis

Yeast cells grown to log phase in YEPD media were fixed in 4% formaldehyde for 30 min at 25°C, and washed three times with PBS. Cells were stained overnight with Alexa Fluor 488-phalloidin (Life Technologies; Grand Island, NY), then washed three times with PBS. To remove actin patches, cells were treated with 100 μM CK666 for 15 min at 25°C prior to fixation. Cells were imaged by structured illumination microscopy (SIM) on a Nikon Ti-2 SIM-E inverted microscope with a Hamamatsu Orca Flash 4.0 camera controlled by NIS-Elements software (Nikon Instruments). Z stacks of images were recorded to capture actin structures across different focal planes, with Z-step of 0.15 um and 7 stacks total. Max projection across all Z stacks per recording was used to generate the final SIM images (examples in Figure 7A). From the SIM images, individual cells were cropped, and actin cables were analyzed using an open source program for biopolymer networks, SOAX.[73] For all SOAX analysis, default settings were used, with two exceptions, to optimize detection of cables: R-threshold value was set to 0.08, and k-stretch factor was set to 0.5. The number of actin cable segments per cell was computed based on the SOAX program output. The size of mother cells was measured in ImageJ using the "oval" selection function.

For the cell imaging and analysis in Figures 7D and 7E, yeast strains were grown to log phase at 25°C in YPD cultures, then fixed in 4.4% formaldehyde for 45 minutes at 25°C. Cells were then washed in 1x PBS (pH 7.3), resuspended in 1x PBS (pH 7.3) + 0.1% Triton X-100, and stained with Alexa Fluor 488-phalloidin (Life Technologies) overnight at 4°C. The following day, cells were washed in 1x PBS (pH 7.3), resuspended with Vectashield mounting media (Vector Laboratories), mounted on slides, and imaged on a Nikon Ti2-E invert confocal microscope equipped with a CSU-W1 SoRa (Yokogawa) and a Prime BSI sCMOS camera (Teledyne Photometrics) controlled by Nikon NIS-Elements Advanced Research software using a 60x, 1.40 NA objective. 3D stacks through the entire cell were acquired at 0.2 μm steps. Images were processed using NIS-Elements Advanced Research software (Nikon). FIJI was used to generate inverted greyscale and maximum projection images. Mother cell area was quantified using the area measurement function in FIJI.

QUANTIFICATION AND STATISTICAL ANALYSIS

All experiments were repeated multiple times, and the number of replicates is reported in the figure legends. Means ± s.d. or s.e.m. were calculated using GraphPad Prism (version 10.0; GraphPad Software, La Jolla, CA), and figure legends specify the n and the error bars (s.d. or s.e.m.) for each experiment. Figure legends also specify statistical tests performed using GraphPad Prism. Differences were considered significant if P value < 0.05 (*), < 0.01(**), < 0.001(***), or < 0.0001 (****), as indicated in figure legends.